DETERMINATION OF THE MECHANICAL PROPERTIES OF GUINEA PIG TYMPANIC MEMBRANE USING COMBINED FRINGE PROJECTION AND SIMULATIONS

By

JUNFENG LIANG

Bachelor of Theoretical and Application Mechanics

Jilin University

Jilin, Changchun, China

2006

Master of Mechanical Engineering

Oklahoma State University

Stillwater, Oklahoma

2009

DETERMINATION OF THE MECHANICAL PROPERTIES OF GUINEA PIG TYMPANIC MEMBRANE USING COMBINED FRINGE PROJECTION AND SIMULATIONS

Thesis Approved:

Dr. Hongbing Lu

Dr. Wei Yin

Dr. David Rubenstein

Dean of the Graduate College

ACKNOWLEDGMENTS

I would first like to express my appreciation to my mentor, thesis advisor and committee chairman, Dr. Hongbing Lu, as well as my other committee members, Dr. Wei Yin, and Dr. David Rubenstein for their advice and helpful comments. I am especially grateful to Dr. Lu for giving me the opportunity to work in the area of Biomechanics with such an interesting and fruitful topic and for giving me free hand in this research.

Additionally, I would like to thank our collaborative group at the University of Oklahoma. They provided samples and technical support during my experiment setup, sample handling and procedures. Especially Dr. Gan, at OU gave me a lot of constructive advices in understanding topic and in the all aspects of the research.

My love and sincere appreciation goes to my parents, Yueqiang and Yunxian Zhang, for raising me and for inspiring me to continue my education. Thank you for teaching me the value of hard work.

I also appreciate the help from Dr. Eann Petterson, who offer a lot technical supports in fringe projection and supply some free software in image processing. It is one of the foundations of my research.

Thanks also to Department of Mechanical and Aerospace Engineering at OSU for their financial supporting during this research. Meanwhile I am grateful to NSF (CMS-0510563) and NIH (NIDCD R01DC006632), for the providing of researching funding.

TABLE OF CONTENTS

LIST OF TABLES

Table Page

LIST OF FIGURES

Figure Page

CHAPTER I

INTRODUCTION

EAR STRUCTURE AND FUNCTION

Contained within the temporal bones, two of the thirty-two bones making up the skull, the ear as an organ of hearing are divided into three parts: the outer ear, middle ear, and inner ear (Figure 1.1). The outer ear contains mainly the ear canal and the outside area of ear canal (pinna or auricle). Formed primarily of cartilage, the human pinna is in the shape of superficial bumps and grooves, which vary from across the population. The ear canal consists of cartilage containing glands and lined with hairs and the rest of the canal is bony, with a tight skin connecting to the outermost layer of eardrum. The middle ear consists of Tympanic Membrane (TM) or eardrum, three small bones named ossicles and the large cavity known as middle ear cavity or tympanum. The structure of middle ear is a chain system terminates at one end with TM and another end with stapes (One of the three ossicles). More detail about middle ear will be discussed in the next section. The inner ear includes both the organ of hearing (the cochlea) and a sense organ that is attuned to the effects of both gravity and motion (labyrinth or vestibular apparatus). The hollow channels of the inner ear are filled with liquid, and contain a sensory epithelium that is studded with hair cells which function as sound sensor. [1, 2]

The outer ear collects sound and funnels the sounds toward the external canal, allowing the sound pressure to excite the TM generating small motion and rotation. The motion and rotation of TM is then transmitted through the ossicles chains to the cochlea. The sound pressure amplified through the ear and, in terrestrial animals, passed from the medium of air into a liquid medium. The stimulated hair cells inside the cochlea then transmit such sound pressure into impulses for nerves by bending of the “hair” (protein filaments).

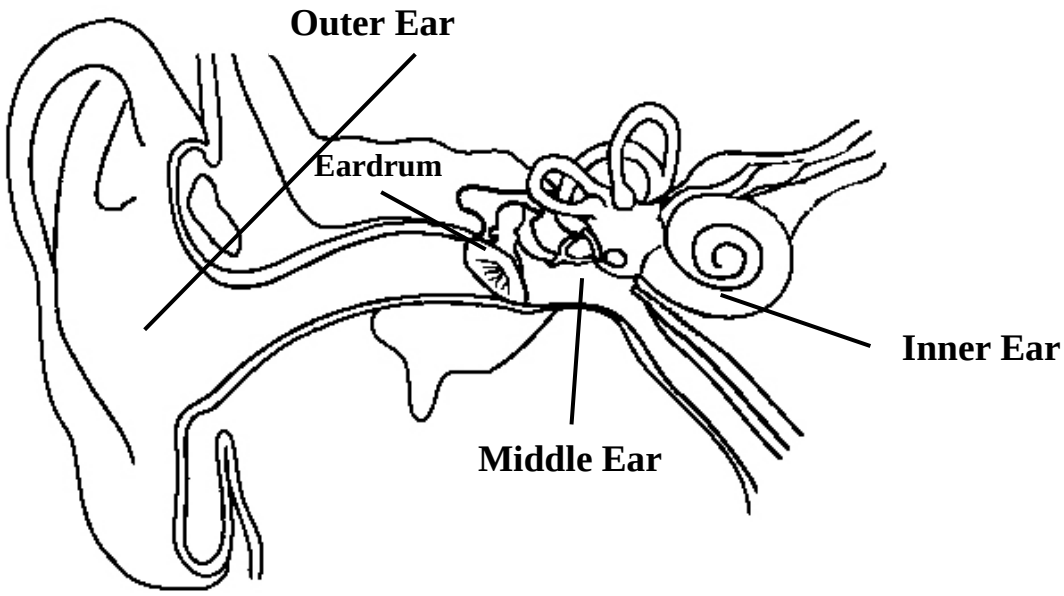

Figure 1.1: Schematic of Ear Structure of Human.

STRUCTURE AND FUNCTION OF THE MIDDLE EAR

The middle ear is separated from the outer ear through TM which receives the sound waves collected by the outer ear and transfers sound vibrations to the middle ear three

small ossicles (i.e., malleus, incus and stapes) and to the inner ear. [3] The TM is a cone-shape membrane with malleus connecting to it in the center, covering about one-third of the area. The malleus has a long process (the manubrium, or handle) that is attached to the mobile portion of the eardrum. The incus is the bridge between the malleus and stapes. The stapes is the last bone that has a structure called footplate connecting to cochlea through the oval window with a structure named footplate (Figure 1.2). These three ossicles are connected to each other as called ossicular chain with ligaments at the joints. The tympanum is not an airtight cavity but with an eustachian tube serving to equalize the air pressure on both sides of the TM.

As is mentioned in the last section, the major function of the middle ear is to provide an effective and efficient way to deliver sound to the inner ear. The first function of the middle ear is to "amplify" the acoustic stimulus. Because the inner ear fluid and tissue are denser than air, the pure air pressure would not be efficient enough to move the fluids and the tissue. Therefore, if driven simply by air pressure, the auditory system would lose some of its sensitivity due to the impedance of the fluid and the structures of the inner ear. Such difference in impedance between air and the fluids and tissues of the inner ear requires a stronger stimulus to be propagated in the inner ear than in air. The lever action of the ossicular chain and the shape of the TM can compensate for this impedance mismatch.

The difference between the effective area of the TM and the area of stapes acts as one of amplification of the sound pressure. For adult human, measurements show that a total

area of 85 mm^2 of the TM is stiffly connected to the malleus. On the other hand, the area of the stapes footplate is about 3.2 mm^2, which is considerably smaller than the effective area of the TM. Consider that if all the force exerted on the TM is transferred to the stapes footplate, then the force per unit of area must be greater at the footplate than the TM. Such increase in pressure can partially overcome the impedance mismatch, and the fluid and tissue in the inner ear can be effectively stimulated [4].

The lever structure of the ossicles also plays a role in transferring force from TM to the stapes footplate. Because the lengths of the manubrium and neck of the malleus are longer than the long process of the incus, the lever action of the ossicular system increases the force impinged on the TM by a factor about 1.3 at the stapes. In addition, the TM tends to buckle due to its conical shape, which causes the malleus to move with about twice the force. The actual pressure transformation depends on the frequency of the acoustic stimulus: generally more effective around about 2 kHz and less effective at low frequency and high frequency. That is why we have a lower sensitivity to sound at low and high frequencies.

Another function of the middle ear is to limit distortion. The muscles in the middle ear serve as “calibrator”, reducing the chance that the acoustic signal is significantly distorted by the middle ear processes. In the middle ear when vibration is large, the pressure of the ligaments may not be sufficient to hold the ossicles together. The tending to separation can distort the transmitted signal at the joint if the contact pressure between the ossicles is smaller than the driving pressure during the vibration. The middle ear muscles assist in

reducing the distortion at high levels, in that they work against one another to press the stapes against the incus, thus limiting the separation and therefore distortion.

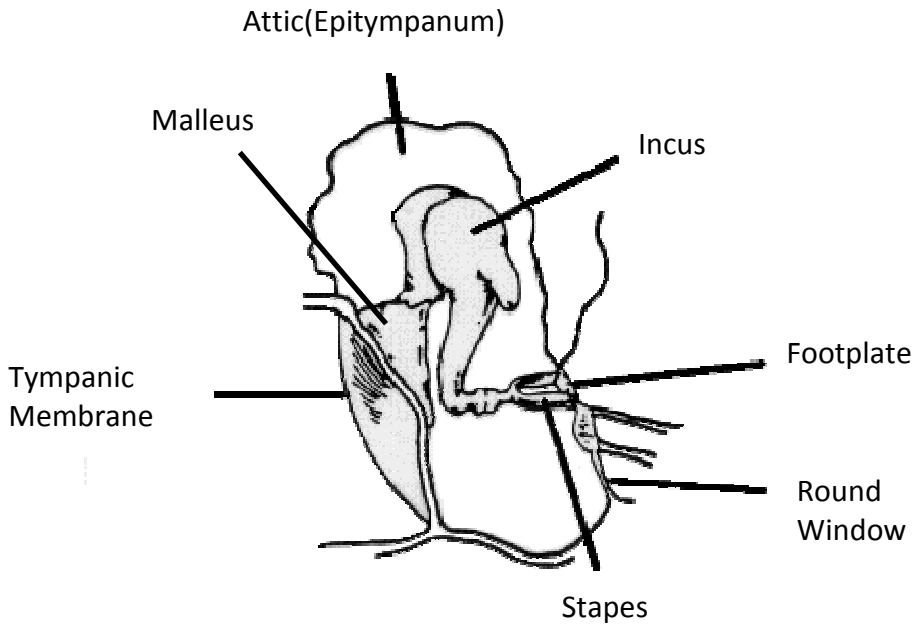

Figure 1.2: Schematic of Middle Ear Structure of Mammals (from Ernest S Campbell, MD, FACS Scubadoc's Diving Medicine Online)

TYMPANIC MEMBRANE

Tympanic membrane (TM) or eardrum is a thin membrane that separates the outer ear from the middle ear located at the termination of the ear canal. Its function is to transmit sound from the air to the ossicles inside the middle ear. Looking from the outer ear to inner ear, the shape of TM is closed to cone, concave outward with about 120^{o} apex, tilting laterally at the top so as to sit in its annulus at an angle of about 55^{o} to the ear canal

(Figure 1.2). The long process of malleus, the manubrium attaches to the TM, located in the middle-ear-side or medial side, from middle top to around the center of TM. The tip of the contact between the manubrium and the TM is known as umbo.

For the convenience of demonstration, two views and four quadrants are defined. The view looking from outer ear to inner ear is called lateral view while the invert direction is called medial view. Divided by umbo, the upper part of the TM is called superior while the lower part of the TM is called inferior. Divided by malleus, the front part of the TM is called anterior while the other part is called posterior (Fig 1.3 (a)).

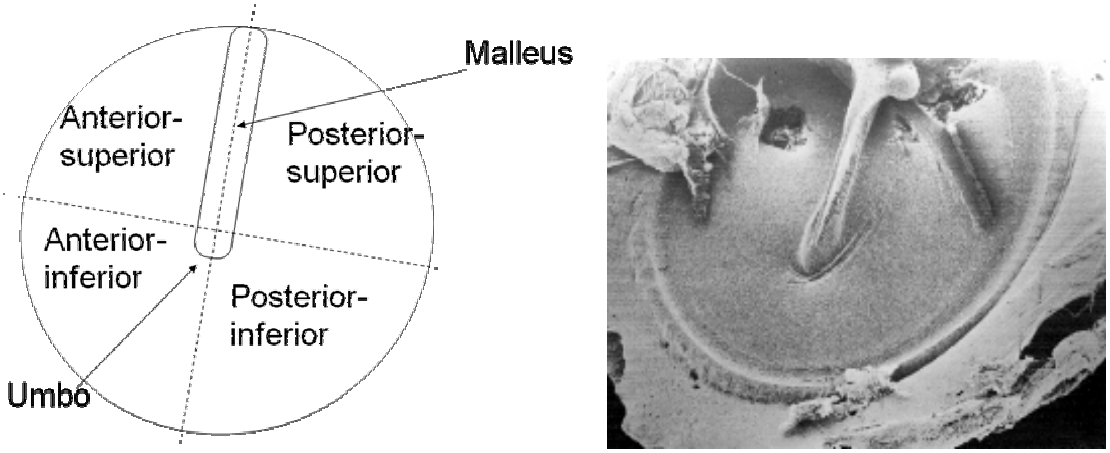

(a) (b)

Figure: 1.3 (a) Schematic of the Four Quadrant of TM. (b) SEM Image of TM in Medial View. (Photographs courtesy of M. Mondain)

The TM is a fiberous composite structure with a cross section consisting of four distinct layers and regions. The layer of TM on the lateral side is called epidermal layer and the most medial layer in the TM is called mucous layer.The outer most lyaer is continuous

with the skin of the ear canal and the most medial layer is continuous with the mucusous membrane of the middle ear. Two layers consisting with colligin fibers lay between the epidermal layer and the mucous layer: a layer of radial fibers just medial to the skin layer, and a layer of cencumfencial fibers between the radial and mucous membrane layers. The entire fiber network is sandwiched between epidermal layer and mucous layer. For most mamals, includeing human, cats, and guinea pigs, the radial curvature of the cone, causing the radial fibers to bow outward toward the outer ear. These radial fibers attach to the annular ring around thte periphery to the eardrum and to the malleus within the interior of the TM. In the human eardrum, the radial fibers encase the malleus near the umbo, providing a very strong attachment to the tympanic membrane to the ossicular chain. The attachment is much losser near the superior end of the manubrium as is shownd in figure 1.4 [5].

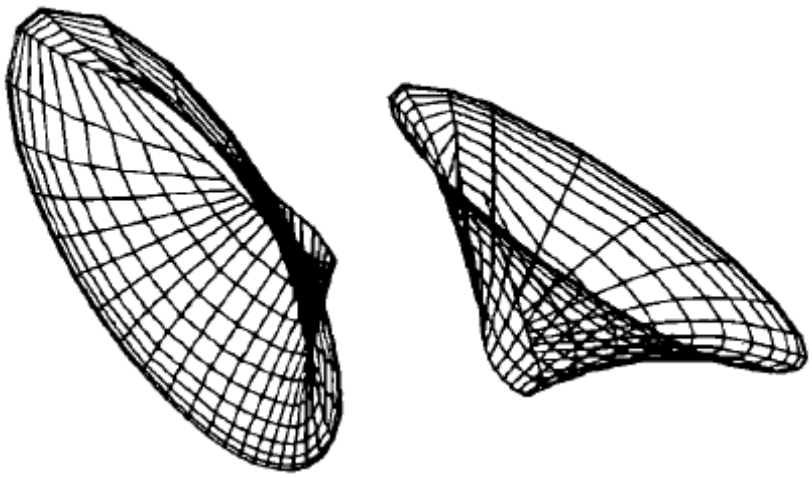

(a) (b)

Figure. 1.4: Geometry of Fiberous Gridwork in TM. (a) and (b) show the geometry used for the cat eardrum.Figure is from reference [5].

MOTIVATIONS AND SCOPE OF STUDY

TM plays a critical role in the function of hearing by vibrating and therefore, it is necessary to measure its mechanical properties. While numerous results have been reported for the mechanical properties, they were obtained from TM speciments cut form TM. In this work, we measure the properties *in vitro* but with intact sample. One way for such a full-field measurement of the mechanical properties of TM is to measure the static properites i. e observing TM mechanical properties under quasi-static pressure.

In fact, rapid external atmospheric pressure changes of several kPa often occur in every day life. For example taking the elevator up in a 100 meter high buiding gives rise to a pressure change of about 1kPa. Static pressures in the middel ear also occur without such changes in exteral pressure. Dishoeck and later van den Bog have shown that negative pressures in some cases down to -2 kPa are often found in normal people. More recent research on gas in the middle ear has shown both positive and negative pressure exceeding 1kPa upon persons awakening in morning. Therefore the inspection of TM mechanical properties under static pressure shows actual values[6].

In order to make a full-field observation, a non-destructive measurement method was used to obtain the mechanical stimulus as pressure. Meanwhile, the mechanical response in this research will be the volume displacement, which is a typical mechanical response being used to correlate to the pressure in TM study. In the following chapters a non-destructive measurement method, fringe projection method, will be introduced to achieve the measurement of the volume displacement. FEM model will be built to further the analysis the mechanical prosperities of TM by combining volume displacement measurement as well as simulation result.

Therefore, it will be the focus for this rearch to meaure, document, and model the mechanical properties of the guinea pig TM. In this work , the hyperelastic properties of the intact guinea pig eardrum are quantified in the form of stress-strain curve through experimental , analytical , and numerical methods. The target of this reserch is to design an method of combined experiments and simulations to obtain a more reliable and more explanable form of mechanical properties description for the entire TM. This method and the data from measurement can further the entire middle ear modeling and provide innovative means to dectect desease on TM.

Guinea Pig TM samples were used in this study. The reason for choosing animal TM is because they are more easily available than human TM. The other reason is that, for the mammals the structures of middle ear and TM are very similar(Figure 1.5), so that the methology develped for measurement of mechanical properties for guniea pig can be used for human TM.

Certain simplifying assumptions msut be made in order to constrain the scope of this work. First, the TM will be assumed consting of uniform material, which is homogenious, isotropic. As a result, the mechanical properties in this work is an estimation over the entire TM. Secondly, the material of the TM will be assumed to be hyperelastic. Although studys have shown that material of TM exhibits viscoelastic bahvior[7,8], the aim of this work is to reveal the hardening effect of the TM under the increase of pressure exerted. Since time-dependent effect is not in interest, hyperelastic model is better to describe such strain-dependent phenomenon rather than viscoelastic model. In a word, these assumptions neither devalue the importance nor limit the usefulness of this thesiss, as elastic models have been shown to yield fruidful use in biomechanic analysis for many years[9-12].

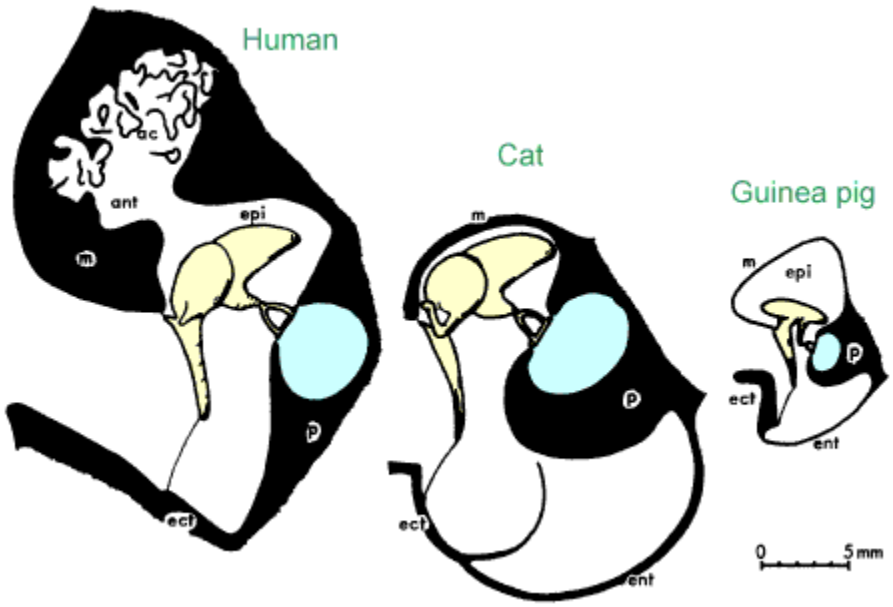

Figure 1.5: Schematic of Different Kinds of Temporal Bones. (Figure from R. Funnell's structure and function of the middle ear site.)

CHAPTER II

BACKGROUND ON FRINGE PROJECTION

MOIRE TECHNIQUE

Moiré patterns are formed by superposition of two regular patterns, typically known as the object pattern and the reference pattern. The most common used pattern is an array of parallel straight lines, which is commonly referred to as a grating (Figure 2.1).

Based on the application of the moiré pattern, there are two kinds of moiré technique. One is in plane moiré; another is out-of-plane moiré. The top two images in Figure 2.1 show the interferometry of two sets of grating. The white and black pattern, moiré pattern, can be used to calculate the position difference between the two gratings. Since in plane moiré is not our interest, it will not be discussed here, the principle to calculate

the displacement field can be found in the work by M. Heredia [14].

The out-of- plane moiré can be used to calculate the out of plane profile thus can be applied as 3-D surface reconstruction. There are four types of out-of plane Moiré methods, they are: Shadow Moiré, Reflection Moiré, Projection Moiré, and Fringe Projection as is shown in Figure 2.2- 2.3.

Shadow moiré is the oldest and simplest technique. As show in Figure 2.2(a), a master grating of pitch p is placed just in front of the object, and is illuminated obliquely so that is casts a shadow onto the surface. When the object is viewed through the grating from a different direction, the interference between the grating and its shadow produces a moiré pattern that contains information about the shape of the object.

Reflection moiré (Figure 2.2(b)) has a similar mechanism, but the specimen must have a polished surface to act as a mirror. A large master grating is placed at a distance h. The camera is set up behind a hole in the center of the object. A first image is collected for the unloaded object, so that the reflected image of point Q in the grating is seen at point P on the object. The object is deformed so that point P in the specimen moves to P', and because the curvature has changed, the image reflected corresponds now to point Q' in the grating. A second exposure is taken, and superimposed on the first image producing a moiré pattern in the double-exposure image, where the fringe order can be related to the slope of the specimen plate.

In contrast with the shadow technique described in the previous section, the projection moiré method requires two different gratings. In the simplest configuration a grating is imaged on the surface of the specimen by means of a projecting lens, and another grating is placed in front of the viewer. Alternatively, the projected fringes can be produced by interference of coherent light.

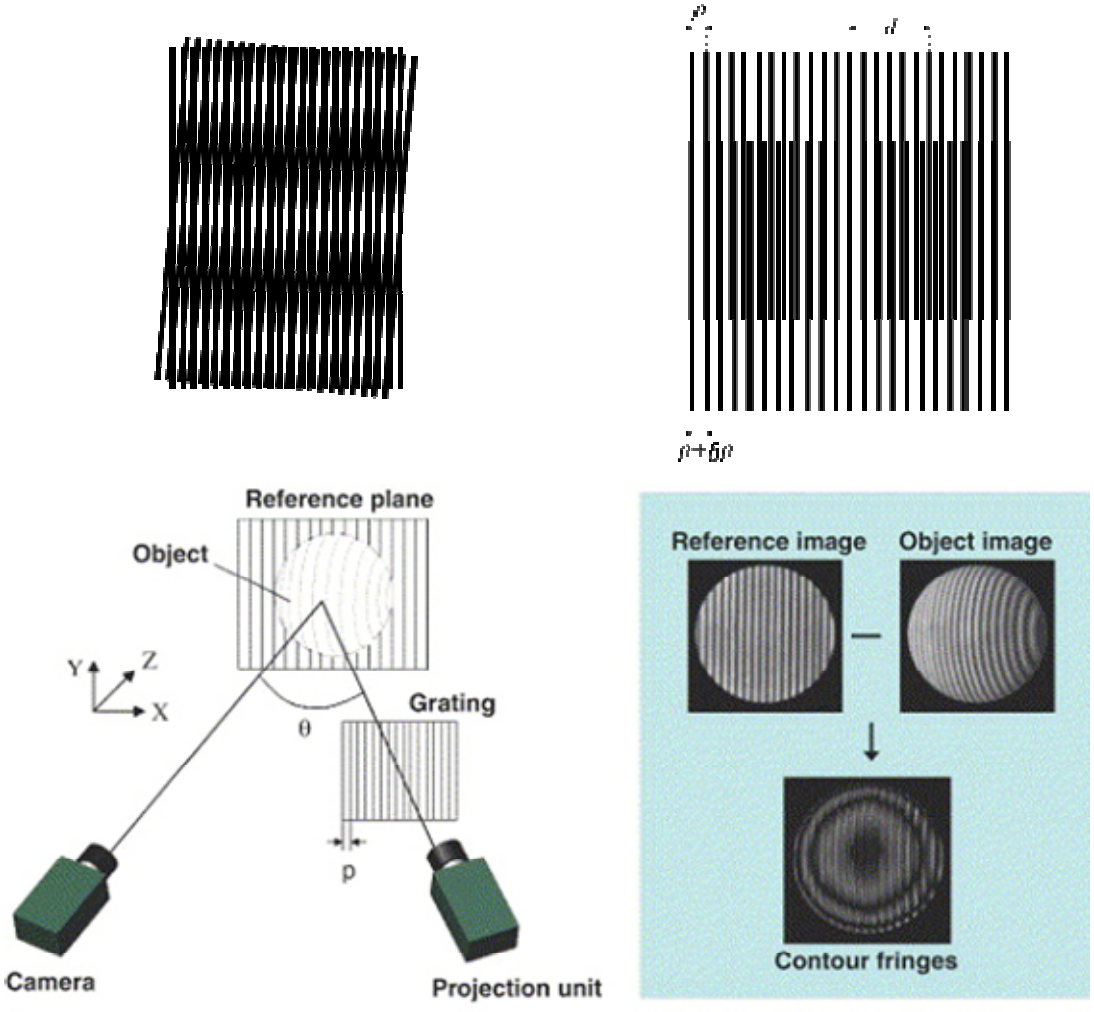

Figure 2.1: Moiré Patterns. Figure from reference [13].

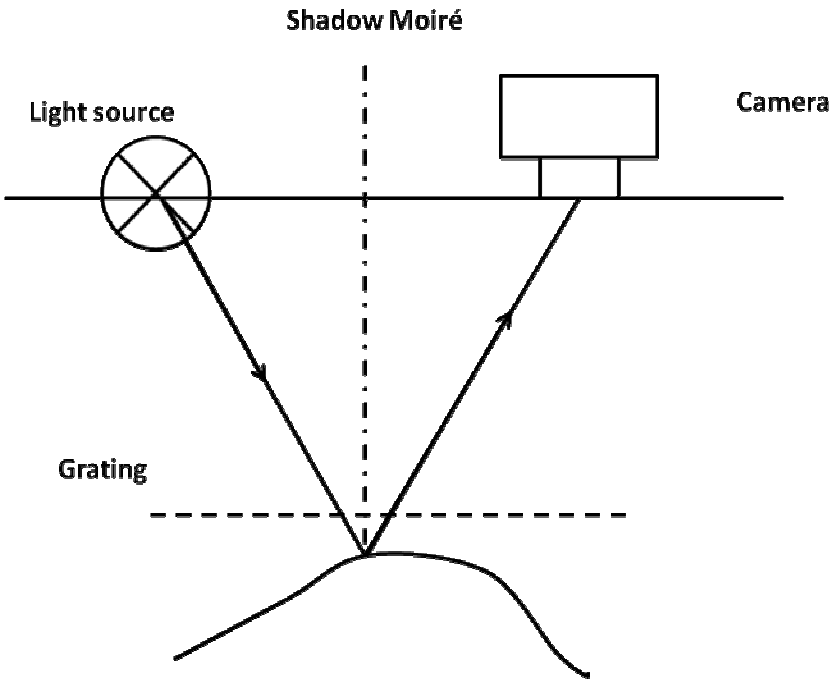

(a)

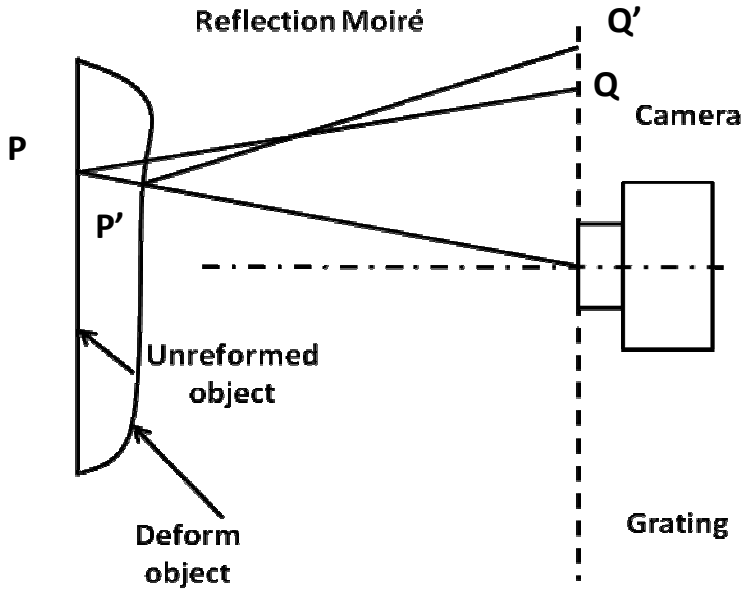

(b)

Figure 2.2: Schematic of Shadow Moiré and Reflection Moiré. (a) Shadow moiré (b) Reflection moiré.

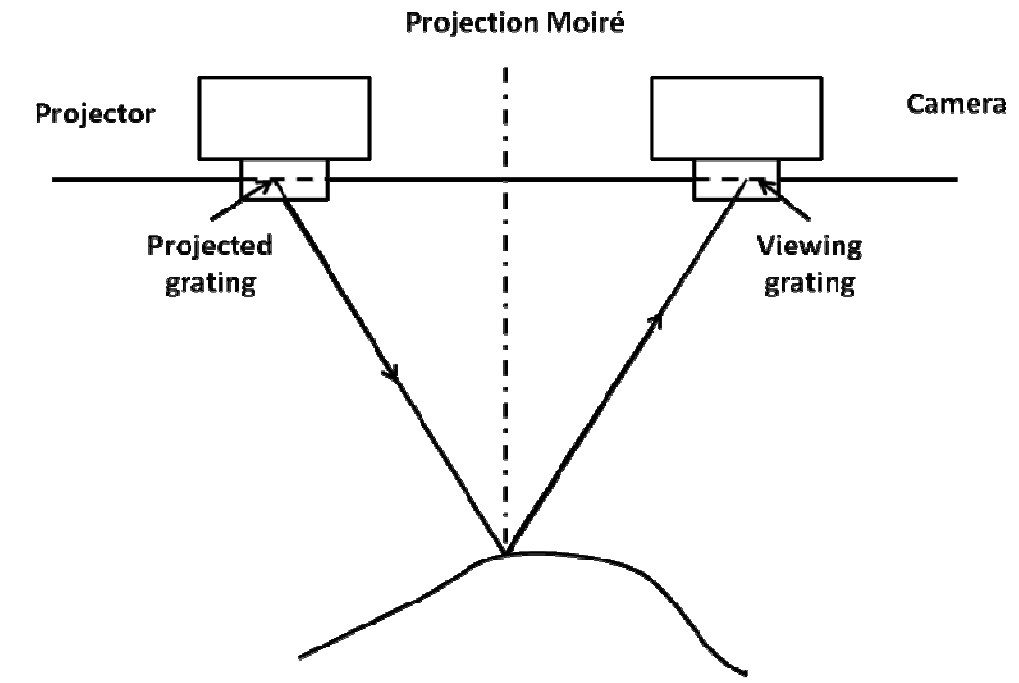

(a)

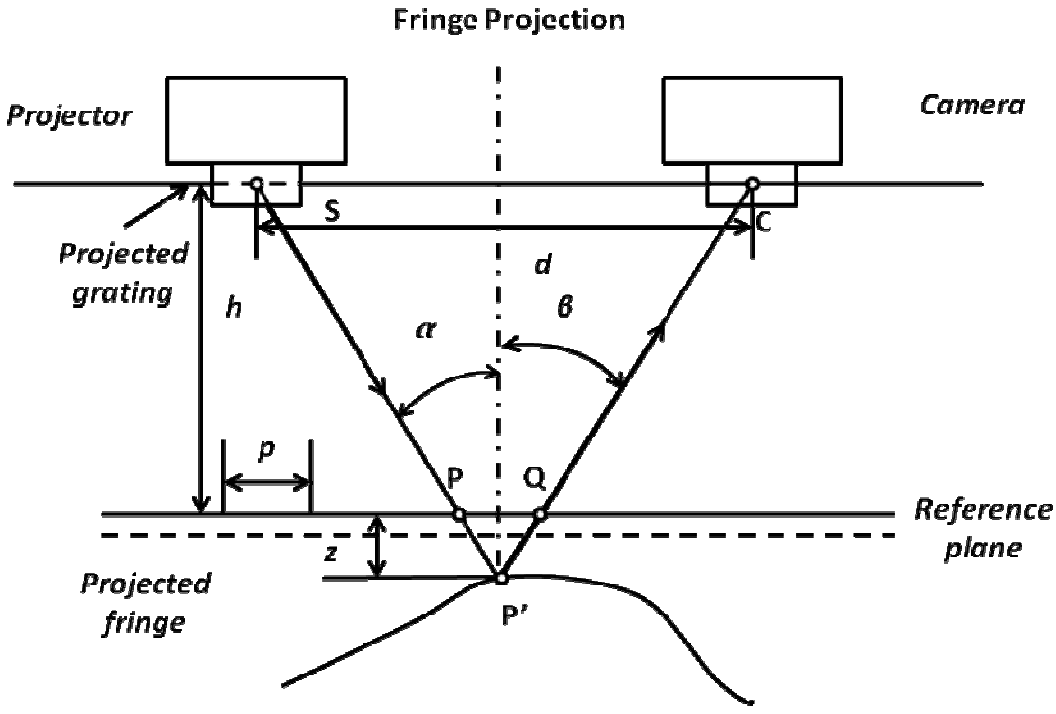

(b)

Figure 2.3: Schematic of Projection Moiré and Fringe Projection (a) Projection moiré (b) Fringe projection.

FRINGE PROJECTION METHOD

The fringe projection technique used in this research also entails projecting a grating onto an object and viewing it from a different direction much like in single projection moiré. Indeed, both methods can be described by a single theory and the fundamental expressions are very similar. The main difference is that the shape information is measured directly from an image of the projected fringes instead of viewing through an analyzer grating to produce a moiré pattern (Figure 2.3).

Such differential measurement of shape can also be achieved by using a double exposure technique-to superimpose two images of the fringes projected onto the specimen in the initial state (*i.e*. the reference image) and final state (*i.e*. the object image). This variation of the technique can be used to measure absolute shape if a flat plate is used as reference, where the fringes represent depth contours (Figure 2.1). The double exposure technique takes advantage of the moiré effect, although without an analyzer grating.

The methods that use the moiré effect generally provide higher sensitivity, because only the moiré pattern and not the grating lines needed to be resolved by the camera, thus finer gratings can be used. However, fringe projection has the advantage that the optics are less complicated and there is no need for accurate matching of the projecting and viewing gratings, providing a very convenient technique for contouring objects. In this work, since the shape of TM is regular and the surface of TM is smooth, considering general information of the entire TM, the volume displacement will be measured, fringe

projection is sufficient to satisfy the contouring of relatively coarse objects. In fact, in section 5 in this charter, it is shown that the measurement for regular shape, the sensitivity of fringe projection is sufficient high even in small scale.

There are two main approaches to digital fringe pattern analysis: intensity-based methods and phase-extraction methods [15]. The intensity-based methods analysis is based on the image intensity distribution alone. By locating the fringe centers, which represent surface contours and assigning fringe order number, a full-field distribution of displacement or height can be determined. However, the drawback of such method is obvious. On one hand, the data is available only at the centers of the fringes; therefore interpolation is required to extract data at arbitrary point in the field of view. On the other hand, in order to determine the fringe order number, priori knowledge is required to distinguish between hills and valleys.

In contrast to intensity-based method, phase-extraction methods constitute a more recent approach to the problem of digital fringe analysis. The aim of these methods is to extract the modulated phase that contains the information encoded in the fringe pattern. This approach is base on the mathematical description of the intensity distribution of the fringe pattern as describe in section 3 in this chapter:

$$I(x,y) = A(x,y) + B(x,y)\cos\left(2\pi fx + \Phi(x)\right) \qquad (2.1)$$

where A and B respectively represent the variation of background illumination and fringe modulation, f is the carrier frequency and the modulated phase Φ is the term related to the

physical property encoded in the fringe pattern. In order to extract Φ from the equation (2.1), temporal phase-shifting techniques are frequently used by means of shifts the master grating with a suitable device. These techniques combine a set of phase-shifted images recorded over a period of time to calculate the phase. The main shortcoming of such technique is the fact that data collection takes place over a period of time and hence unsuitable for transient application.

In contrast, a second group of techniques known as spatial phase shifting enable the collection of data of shifting simultaneously. The phase can be processed in frequency domain using Fourier transform. The disadvantage of spatial phase shifting is the very involving of computer and the loss of resolution in the direction of the phase shift because of the averaging over a fringe period. Meanwhile, the spatial techniques have difficulty dealing with discontinuous patterns such as shapes with steps.

In this work, considering the regular geometry of the TM and the requirement of recording the entire surface information, the volume displacement, phase shifting on singe image technique will be used. The further detail will be discussed in the next section.

THEORY OF 3-D PROFILE RECONSTRUCTION

In this section the theory of 3-D surface topography reconstruction for fringe projection will be described. It is similar to projection moiré theory.

Considering both telecentric (i.e. viewing and observation at infinity) and non-telecentric cases, a schematic diagram of the elements in a typical fringe projection system is shown in Figure 2.4. A master grating G with pitch p_0 is projected onto the object using lens $\mathbf{E'_p}$-$\mathbf{E_p}$. A camera records the images of the fringe pattern projected onto the object through lens $\mathbf{E'_c}$-$\mathbf{E_c}$. The camera is aligned perpendicular to the reference plane at a distance h while the projector is aligned at a distance d away from the camera. The optical axes of the projector and camera lie on the plane of the figure and intersect at point **O**. The coordinate system xyz was chosen with origin at **O,** z on the camera axis, x on the plane of the figure and y normal to the figure. The reference plane is located at z=0 plane.

If a telecentric projector is used (denoted as $\mathbf{E}_\infty$ in the figure), the gratings projected onto the reference plane as fringe with constant pitch of frequency $f = 1/p = cos\alpha/p_0$. If the transmission function of the grating is sinusoidal, the intensity of the image seen by the camera can be described as

$$I(x,y) = \frac{1}{2}(1 + \cos(2\pi f x)) \qquad (2.2)$$

If $\mathbf{E_p}$ is at a finite distance i.e. in non-telecentric case, the image of grating will be x dependant which can be described as

$$I(x,y) = \cos(2\pi f(x + s_0(x))) \qquad (2.3)$$

where

$$s_0(x) = (\overline{\mathbf{BC}}) \tag{2.4}$$

where **B** is the point that is projected onto the reference plane from a telecentric projector and **C** is the counter point that is projected from a non-telecentric projector. For convenience, we can express light intensity as

$$I(x,y) = \cos\,(2\pi f x + \Phi_0(x)) \tag{2.5}$$

where

$$\Phi_0(x) = 2\pi f s_0(x) = 2\pi f \overline{\mathbf{BC}} \tag{2.6}$$

For arbitrary surface, the gratings projected onto the surface point **H** will be seen as point **D** on the reference plane. The deformed grating can be described as

$$I(x,y) = A(x,y) + B(x,y)\cos\,(2\pi f(x + s(x))) \tag{2.7}$$

where $A(x,y)$ and $B(x,y)$ are, respectively, the background and the modulation terms that models an arbitrary distribution of reflectively ion the object surface. Similarly, we can simplify (2.7) as

$$I(x,y) = A(x,y) + B(x,y)\cos\left(2\pi f x + \Phi(x)\right) \tag{2.8}$$

where

$$\Phi(x) = 2\pi f s(x) = 2\pi f \overline{\mathbf{BD}} \tag{2.9}$$

Note that $\mathbf{E_pHE_c}$ and **CHD** are similar triangles, therefore

$$\overline{\mathbf{CD}} = \frac{zd}{h-z} \tag{2.10}$$

And

$$\overline{\mathbf{CD}} = \overline{\mathbf{BD}} - \overline{\mathbf{BC}} = \frac{\Phi(x)}{2\pi f} - \frac{\Phi_0(x)}{2\pi f} = \frac{\Delta\Phi(x)}{2\pi f}$$

(2.11)

Combining (2.10) and (2.11) and substitute f, we have

$$z = \frac{\left(\frac{\Delta\Phi}{2\pi}\right)ph}{d - \left(\frac{\Delta\Phi}{2\pi}\right)p}$$

(2.12)

If the projection is telecentric i.e. $z/h << 1$ and $p/d << 1$, (11) can be approximated as

$$z = \frac{hp}{d}\frac{\Delta\Phi}{2\pi}$$

(2.13)

From equation (2.12) and (2.13) we can see that in order to extract the height information, we have to obtain the phase terms Φ of both object image and reference image. A phase measurement method using five step spatial algorithm used to implement the extraction can be express as

$$\Phi^* = \arctan\left(\frac{2(I_2 - I_4)}{2I_3 - I_5 - I_1}\right) \qquad (2.14)$$

where I_i i=1,2,3,4,5 denote shifts of the image in the direction perpendicular to the

fringes

$$\begin{cases} I_1 = I(i, j - int(p/2)) \\ I_2 = I(i, j - int(p/4)) \\ I_3 = I(i, j) \\ I_4 = I(i, j + int(p/4)) \\ I_5 = I(i, j + int(p/2)) \end{cases} \tag{2.15}$$

where p represents the pitch of the reference image while the above expressions are applied to both object and reference image. The pitch is calculated from 1-D FFT of all rows of the reference image, by removing the DC component and averaging the first peak of all the rows.

As is shown in equations (2.8) and (2.14), the phase terms are apparently wrapped within the interval $[-\pi, \pi]$, and presents 2π discontinuities at the end of the periods. Many phase unwrapping technique are available to compensate the multiples of π until a continue phase map is obtained. A simple approach to the problem is to detect these jumps and add appropriate multiples of 2π to the wrapped phase until it is made continuous. However, the implementation of this simple method in reality can be problematic due to the noise and the singularities that may create false jumps. In two or more dimensions, the unwrapping process is path-dependent. The wrapping method we used in this thesis is the quality bins algorithm, of which free unwrapping software is available on Dr. Eann Petterson's experimental mechanics website. The details of the quality bins unwrapping algorithm can be found in reference [16].

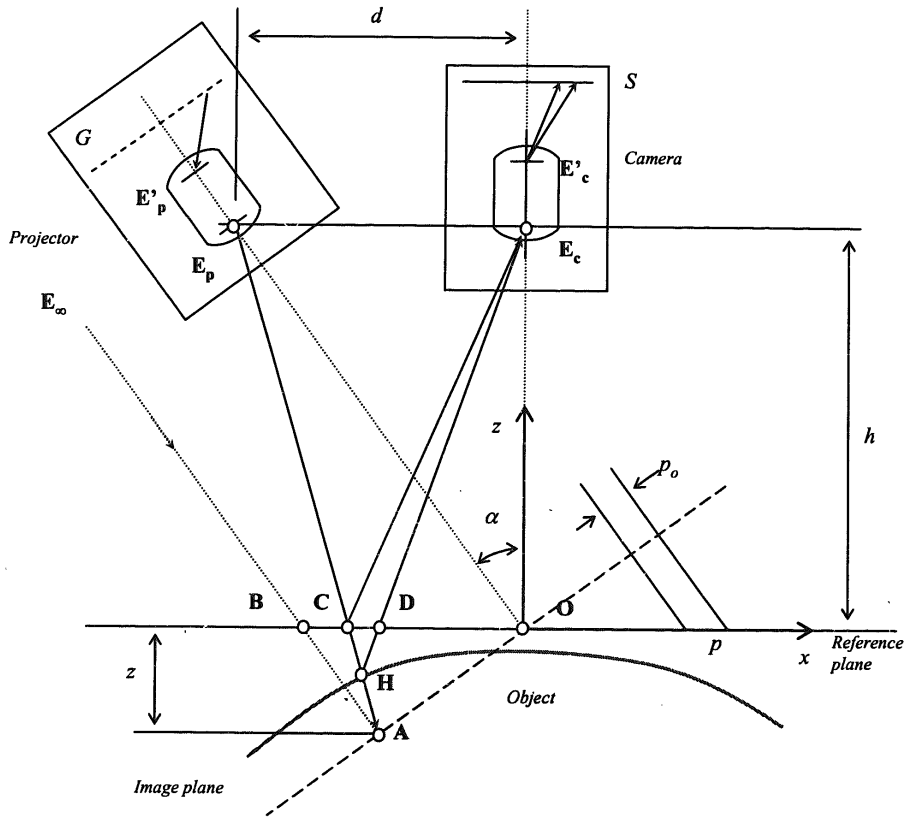

Figure 2.4: Schematic of Optical Configuration for the Fringe Projection Method. The figure is from reference [14].

CHAPTER III

PREVIOUS STUDIES ON MECHANICAL PROPERTIES OF TM

CUT-OFF-SAMPLE-BASED MEASUREMENT

The measurement of elastic modulus of TM by cut-off sample can be track back to as early as 1960. Von Békésy first presented his bending test of the dissected tongue-shape TM strip with Young's modulus of TM as 20 MPa [10]. Kirikae measured the Young's modulus of TM through longitudinal dynamic test on the TM strip with reported modulus of 40 MPa [9]. Decraemer et al. conducted tension test and reported modulus of 23MPa [11]. Cheng et al. reported the in-plane Young's relaxation modulus as a function of both time and stress on the TM specimens cut primarily along the circumferential direction of a TM [17]. More previously, Luo provided a technique to measure the mechanical properties of TM at high strain rates using a miniature split Hopkinson tension bar. The TM samples were cut into strip for a dynamic loading up to half of a newton. The results are reported as 45.2-58.9 MPa in radial direction and 34.1-56.8 MPa in the circumferential direction [3, 18].

In that TM is an inhomogeneous structure with anisotropy in radial, circumferential, and through-thickness directions, methodology to characterize viscoelastic relaxation modulus in different direction and location is more recently come into interest. Huang et al. established methods for measuring linearly viscoelastic properties of human TM using nanoindentation. Results were reported relaxation modulus of TM in both wet as well as dry condition with emphasis on the measurement technique on the wet specimen. Later on, statistical form of properties was reported by Nitin et al. using nanoindentation in four quadrants of human TM. The results are compared between in-plane measurement and through-thickness measurement [8]. Although in use of the entire TM, the samples were cut off from temporal bone with removal of the malleus.

Generally, these cut-off-based measurements of mechanical properties of TM can be also catalog based on the experimental approach: measurement under the static and quasi-static test (Von Békésy, 1960; Luo, 2008), or measurement with dynamic test (Kirikae, 1960; Decraemer et al., 1980; cheng et al., 2007; Huang et al., 2008; Nitin et al., 2008).

No matter what kinds of catalog it is, each of the cut-off-based experiment requires the dissection of the TM from the temporal bone. The major drawback of this method is that the cutting could compromise the eardrum's structural integrity and alter its mechanical properties. As discussed in chapter II, the TM is composed of sandwich-structure layers with the epidermal layer continuous to the canal and the mucosal layer continuous the middle ear cavity. Thus the TM in reality is under certain type of strain when remaining attach to the annular ring of the temporal bone. The bending of the radial collagen fiber in

the lamina layer also indicates the pre-stress on the TM before cutting off. Meanwhile, data in literature (Figure 3.1) has shown that, there is hardening effect when the TM is under high strain, revealing hyperelastic properties. The pre-stretch state of the TM in its *in vivo* state as well as the hardening property of the material composing the TM shows that the cutting of the sample can do harm to the revealing of mechanical properties of the TM, and thus cut-off-based measurement has limitation in reliability to some extent.

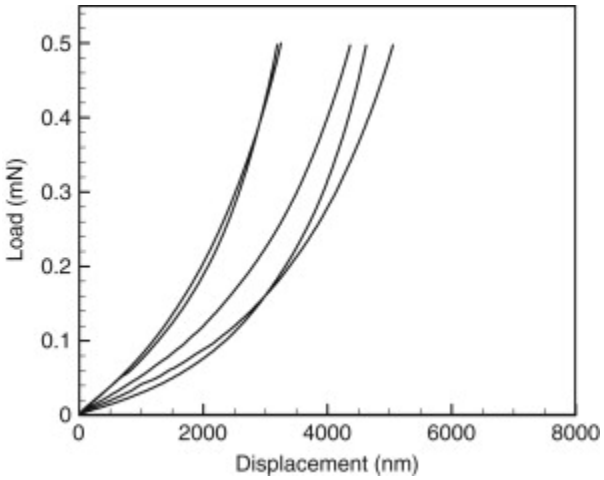

Figure 3.1: Load-displacement Curves from Out-of-plane Nanoindentation Tests. The figure is from reference [8].

FULL-FIELD MEASUREMENT

Full-field measurements of TM constitute another approach for investigating relatively "macro" mechanical properties of the TM retained intact within the temporal bone. These methods usually provide pressure as mechanical stimulus and the observation of the

entire TM changes-for example, Shape, vibration mode, and volume displacement- as mechanical response.

The early studies on the full-field mechanical observation of the TM are primarily in use of tympanometry (a compacted apparatus consisting of tube microphone, sound source and monometer) but the data of the displacement of the TM are hidden in papers on tympanogram [19, 20]. There is no full field quantitative data on the deformation of the TM until 1990, Dirckx et al., presented static pressures measurement on fresh human temporal bone using a non-contacting optical technique, phase shift moiré topography. The full-field deformation of the TM under different quasi static states was presented; umbo displacement and rotation angle of manubrium was compared with other work [6]. Von Unge et al. later on analyzed mechanical changes in different parts of the TM in their full-field study on gerbil TM under static pressure variations using real-time differential moiré interferometer [21]. Hysteresis effect was found in the displacement under identical pressure gradients during the loading and the unloading phase. Their further full-field TM study then moved on to the disease analysis as otitis media effusion and the comparison the TM responses to static pressure with mobile malleus and immobile malleus [22, 23]. In spite of full-field investigation of TM in either topography or middle ear cavity volume change, none of these work provided any parameters of traditional mechanical properties such as modulus.

More recently, *in vivo* areal modulus (AM) of elasticity was measured, and the middle ear mechanical function was modeled by Gaihede et al. [24]. They introduced a method to

measure *in vivo* volume displacement of human TM under pressure using tympanometry. At the mean time, by comparing various clinical conditions, he found that secretary otitis media with middle ear effusion results in significantly hysteresis (Figure. 3.2). With an analytic model of TM as a flat circle membrane before deformation, Gaihede was able to provided mechanical properties in the form of average over the area as areal modulus. The *in vivo* estimates of Young's modulus was hence obtained and reported about a factor 2-3 smaller than the data found *in vitro*. Albeit as the first work that estimate mechanical properties with full-field measurement mechanical response of TM, the reliability of the estimation was compromised by the over-simplified TM model--as discussed in chapter II, in reality, the TM is a concave cone with a 120^{o} angle.

The major shortcomings of the mentioned full-field investigation of TM is that the mechanical behaviors of TM are mostly described qualitatively rather than quantitatively in view of mechanical parameters. Despite the use in specialized applications such as disease detection or modal analysis, the mechanical behavior of material is blurry and the data are generally difficult to be used for the intact middle ear model.

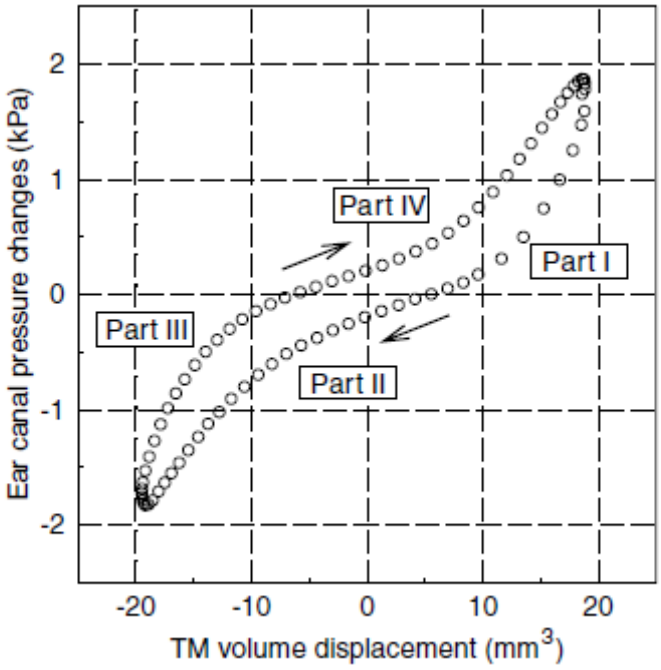

Figure 3.2: The Standardized Pressure-volume Relationship. The figure is from reference [24].

OTHER STUDY ON TM

As discussed in chapter II, the function of the middle ear is to resolve the acoustic impedance mismatch between the air in the ear canal and the fluid in the middle ear.

Without this impedance matching, very little acoustic energy would be absorbed into the cochlea. The first step in this process is the TM converting sound in the ear canal into vibration of the ossicles. Many of researches have been focus on understanding how the TM manages its task so successfully over a broad frequency range.

Hunter et al. used video otoscopy to closely inspect TM pathology and pioneered in measurement of the transfer function of middle ear in 1997 [25]. Susan et al. later on measured the four response variables of sound transmission through the middle ear with acoustic stimulation at the TM [26]. The relation between cavity pressure and the impedance at the TM was shown. Gan et al. measure the human middle ear transfer Function using a double laser interferometry system. Displacement of TM, incudostapedial joint, and stapes footplate induced by sound pressure in the ear canal were simultaneously recorded in both amplitude and phase [27, 28].

In these studies, TM was considered as one of the functional components of the middle ear in compensating acoustic mismatch, where impedance and transfer function of sound pressure over frequency range were measured. However of the mechanical properties of TM alone could provide a better understanding of how the sound pressure was transmitted from TM to ossicles. Therefore, measurement of mechanical properties of TM can be supplementary to sound transmission study for middle ear.

CHAPTER IV

EXPERIMENTAL METHOD

SAMPLE PREPARATION

7 fresh-frozen, guinea pig temporal bone or bullas obtained through University of Oklahoma Health Sciences Center were used in this study. Before experiment, the stored bullas were unfrozen by immersing the sample into 0.9 % saline solution (0.9% NalCl, PH 5.6) for 30 minutes. The ear canals were opened with dental high speed drill to expose the whole surface of TM. Special care was taken no to damage the epithelial layer which is continuous lining the external ear canal. A ventilating hole of about 3 mm diameter was drilled into the middle ear for the exerting and measurement of air pressure. A PVC tube with 2 mm outside diameter was plugged into these holes and the surface of bulla was tightly sealed with Vinyl Ploysiloxane and super glue to prevent leakage from eustachian tube. Since the surface of the guinea pig TM is translucent, in order to obtain clear images of the fringe pattern, the TM was dyed with light reflecting material (Chinese white ink) to give a good visual access to the CMOS camera (Figure. 4.1). To prevent the risk of damaging the TM by the chemicals and to defer the dehydration of TM surface, almond oil was blended with the dying materials. The samples were then checked for complete sealing by applying pressure loading up to 200 Pa and observing a stable level of reading from monometer. The detail about pressure loading will be

described in the next section.

Since vertically projection image of guinea pig TM on to a plane is closed to an ellipse, in order to compare with the FEM model, and validated the reconstruction of the TM, the dimension of TM samples was measure with vernier caliper in two directions: Superior-inferior direction and anterior- posterior direction. The data of the 7 samples is listed in Table 4.1.

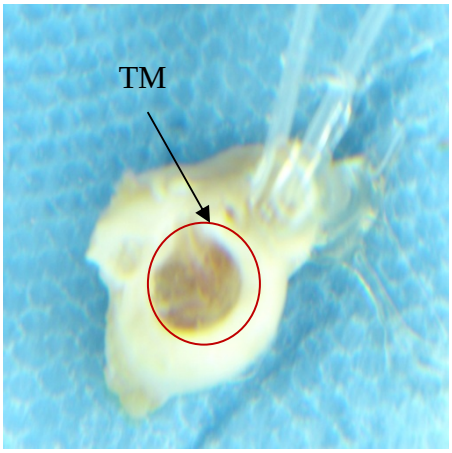

Figure 4.1: Typical Guinea Pig Bulla Sample and Preparation. The tubes shown in the image was used to apply and measure air pressure inside the bulla.

Sample	Ear	Superior-inferior Diameter(mm)	Anterior-posterior Diameter (mm)
GP-08-2-09	Right	5.192	4.605
GP-08-2-09	Left	5.134	4.222
GP-08-5-3L	Left	4.783	4.675
GP-08-5-1L	Left	5.084	4.349
GP-08-5-2L	Left	5.124	4.743
GP-08-5-4R	Right	4.986	4.42
GP-08-5-1R	Right	5.108	4.821

Table 4.1: Dimension of Bulla Samples.

EXPERIMENTAL SETUP

Figure 4.2 shows a schematic drawing of the fringe projection setup and the pressure loading system for the measurement of the mechanical properties of guinea pig TM. The experimental setup can be divided into three sections: the sample holder, the fringe projection system and the air pressure system.

A custom-remodeled temporal bone holder for guinea pig bulla was used to provide two degrees of freedom in rotation for the guinea pig bulla (Appendix A). After mounted on

the temporal bone holder, the direction of the guinea pig bulla can be adjusted to ensure that the convexity of TM surface was perpendicular to the axis of the camera in the fringe projection system. This alignment was required for the determination of the malleus location in the FEM model construction through TM image. It also enabled sufficient and even illumination from the fringe projector to the TM surface, reducing shallow of canal. An assembly of *X, Y, and Z* translation stage (Velmex A60 series) held the temporal bone holder providing three degrees of freedom translation to position the specimen exactly within the field of the projected fringe as well as the fields of view of the camera.

A CMOS camera (XS-4 X-Stream Vision) was mounted on a surgical microscope (Carl Zeiss OPMI-1B) with a 75% beam splitter (Carl Zeiss 75) which was 250 mm perpendicular away from the sample holder plane. A custom-made fringe projector was located 88 mm away from the microscope and this provided an angle between microscope-camera assembly and projector as about 19.3^{o}. From equation 2.13 we can see that, the combination of a fine grating and a small angle generally produces better results than larger angles and coarser gratings for a given level of sensitivity. In [14], it mentions that the distance of the instrument should be at least one order of magnitude larger than the size of the object. In our experiment, guinea pig bulla is about 25 mm; therefore such arrangement satisfies the telecentric condition so that equation (2) can be used.

The projector consists of a 100 W fiber optic lamp (Carl Zeiss), two collimation lenses, a grating and an object lens (Figure 4.4). The focus lens of the object lens is adjustable so

that a sharp pattern with equal pitch for black and white fringes was projected onto the reference plane and the object. The collimation lenses filter the light from the fiber optic lamp so that the noise from light source is damped. The grating we used were with a square wave transmission profile called Ronchi rulings (Edmund Sc. Co.) with pitch density of 20 cycle/mm [29]. In order to satisfy sinusoidal transmission profile condition without more complexity, we purposefully allowed the camera to be slightly out of focus when taking the image, after a sharp focus distance was determined [30].

The air pressure system was composed of a syringe, a U tube monometer and a 3-way stopcock air regulator. The air pressure was generated by moving the piston of the syringe, while the pressure level was control by combining the monometer and the air regulator: once the air pressure reached required level, the regulator was closed and the pressure level was maintained. The air pressure was conducted with PVC tube with Christmas-tree-shape connector to ensure airtight condition when the tube in the guinea pig bulla was connected to it.

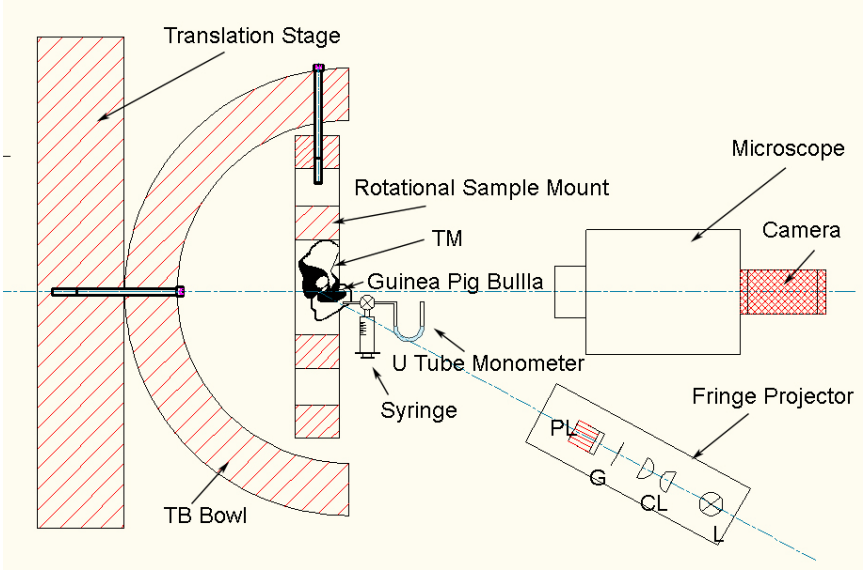

Figure 4.2: Schematic of the Experimental Apparatus. On the right top, the custom-made fringe projector includes: projection lenses P**L,** gratings **G,** collimation lens **CL, Experiment setup** and fiber optic lamp **L.** On the right bottom are the microscope and the camera. On the right hand side is the sample holder on the translation stage with sample connected to the air pressure source and the U-tube monometer.

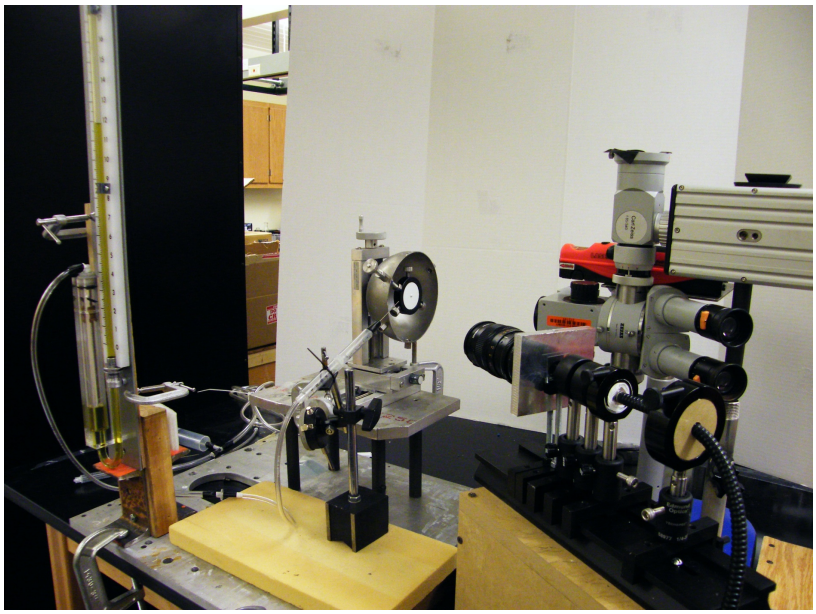

Figure 4.3: Experimental Setup.

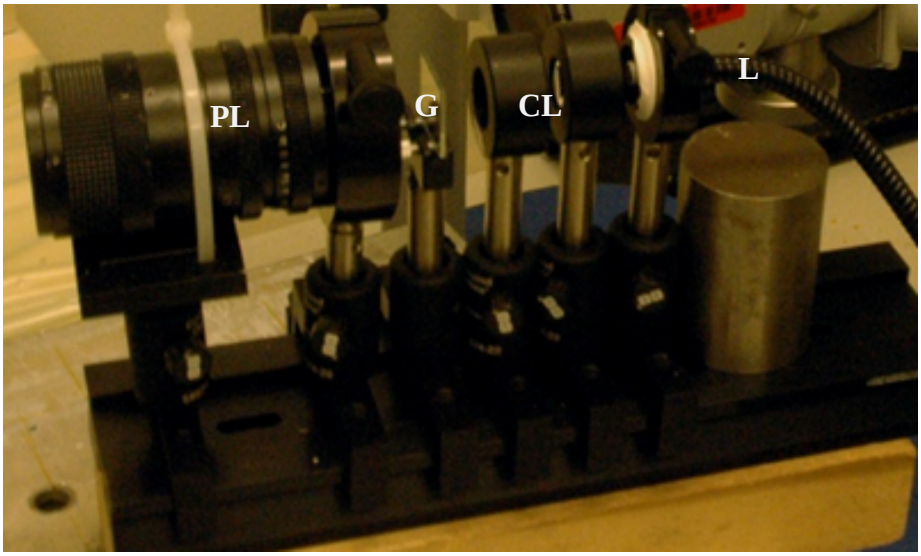

Figure 4.4: Custom-made fringe rojector consists of: projection lenses P**L,** gratings **G,** collimation lens **CL, Experiment setup** and fiber optic lamp **L.**

EXPERIMENTAL PREPARATION

(a) Calibration for The Arrangement Parameters

In equation 2.4, it has shown that the depth map is related to setup arrangement parameters h, and d while these parameters, practically are difficult to directly measured. A calibration by analyzing a surface of known geometry was used to remove the need for making direct measurements of these parameters [31]. A flat reference, an aluminum plate with glossy paint, was position in front of the specimen, and aligned perpendicular to the viewing axis of the camera using the alignment laser mounted on the camera. A reflection mirror was mounted at the end of the plate to reflect the laser beam. The

orientation of the plate is adjusted so that the reflected beam is aimed back at the laser source to ensure the correct alignment, and the plate was fixed in position. The fringe projector is switched on to collect the reference image.

A calibration cone with known geometry (height and diameter) was attached to the reference plate and second image is recorded. The size of the cone is selected to approximately match that of the features of interest in the sample.

The two images were processed to extract and unwrapped the modulated phase map using the processing algorithms described in chapter III. By comparing the phase map with the known geometry, the d and h can be determined. Figure 4.5 shows the cone and the reference plate used for calibration. The cone has a height of 2.3 mm height and a width of 6mm width, mounted on the reference plane, an aluminum plate with galvanization paint.

Figure 4.5: Calibration Cone for Obtaining Arrangement Parameters.

(b) Validation of the Fringe Projection Setup

In order to validate the height measurement of the fringe projection setup, another validation cone with 2.5 mm height and 6.25 mm diameter was measured in the system with the same procedure as in the previous section and the identical arrangement

parameter from the calibration. An average error of 0.2% was observed in the z direction and an average error of 0.72% was observed in radial direction in plane. Figure 4.6 shows a typical reconstruction image of the validation cone.

The validation shows that the miniature fringe projection system is able to achieve a reliable resolution and accuracy for small object as guinea pig TM.

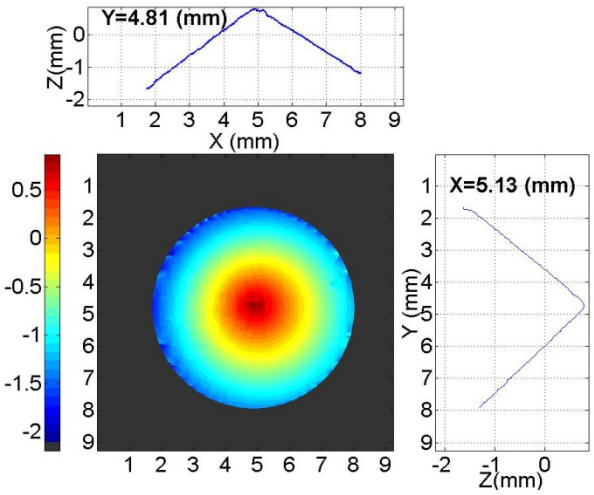

Figure 4.6: Typical Reconstruction the Validation Cone.

(c). Image Preprocessing

Although the guinea pig TM was fully exposed from the ear canal, the continuity between the epithermal layer and the canal skin requires the remaining of the annular ring and its bony boundary. With optimal arrangement, the shadow of the canal can still affect the quality of the image by uneven illumination and thus induce errors. Since only the

phase is of interest, a normalization procedure was applied to unify the background illumination and the modulated illumination (see equation 2.1) [31].

1. Divide the intensity map I in M_k x N_k blocks. The block size should be larger than the pitch so as not to distort the signal, but sufficiently small to follow the variation of the amplitude and the background terms. An empirical expression that provide good results in practice was$\{M_k\ N_k\}$=min(1,5p, $\{M, N\}$/60), where p is the pitch of the fringes and M, N the image size.
2. Estimate the back ground term A^*: (i) calculate the average of each block, to estimate the background term at its center, and (ii) fit a smooth polynomial function through the calculated values to extrapolate them and generate a smooth map of the background the same size of the original image, *i.e.* A^*=extrapolate (mean (blocks (I))).
3. Estimate the modulation term B^*: (i) subtract the calculated background map A^* from the original intensity map I, (ii) calculate the difference between the minimum and maximum value of each block, and (iii) extrapolate as above to yield a smooth map of modulation, *i.e.* B^*=extrapolate(max(blocks(I- A^*))-min(blocks(I- A^*))).
4. Compute the normalized the image by removing the two terms previously calculated from the original intensity map, *i.e.* N= (I- A^*)/B^*.
5. Re-scale the normalized image to the desired range of intensity(typically 0-255).
6. Apply a smoothing filter to remove noise from the image, usually either the

median or the mean filter.

The effect of this normalization algorithm can be seen in figure 4.7, and the program of the algorithm can be seen in appendix B.

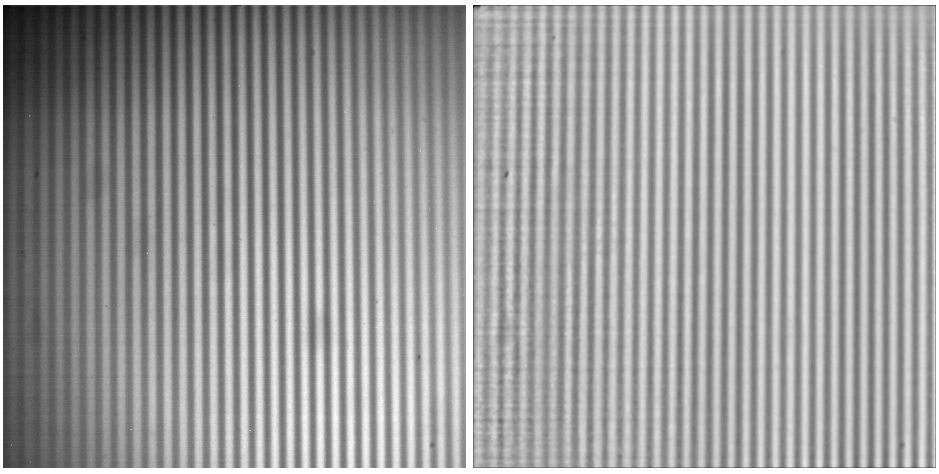

(a)

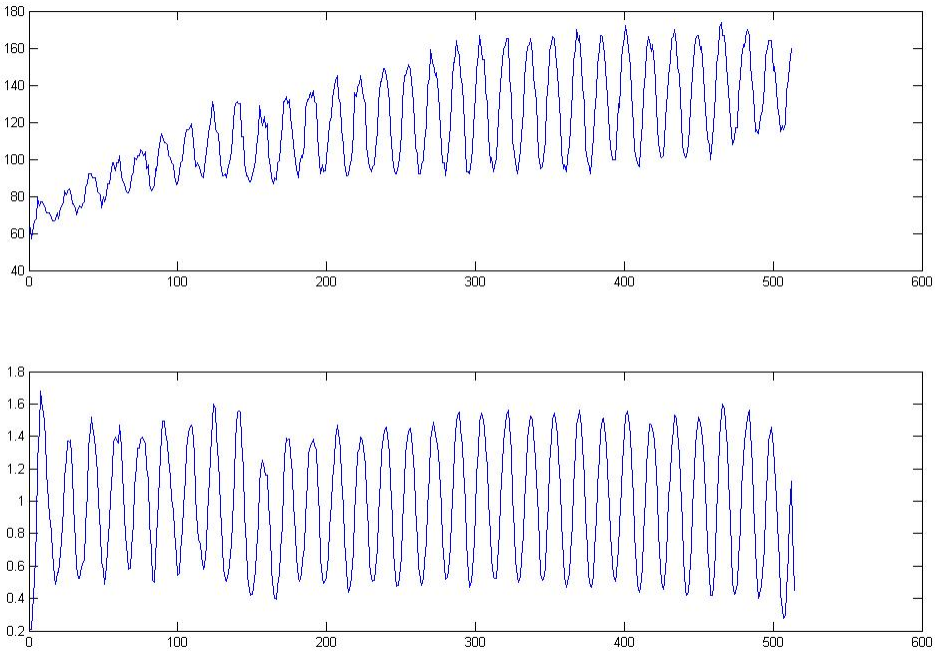

(b)

Figure 4.7: Normalization for Image Preprocessing. (a). Image of fringe projected on a flat plane. Picture on the left hand side shows the original image, and on the right hand side shows the image after normalization (b). The plots on intensity profiles along a line in (a). The plot on the top shows the original intensity distribution, while the plot on the bottom shows the intensity after normalization.

EXPERIMENT PROCEDURE

As is shown in Figure 4.2, the prepared guinea pig bullas samples were securely mounted on the temporal bone holder. The tubes as described in the previous section were connected to a 3 way stopcock which has three direction connection fluid controls. A syringe to add pressure to the sample and a U- tube monometer to measure pressure were connected to the stopcock.

Each specimen was preconditioned through applying pressure by 4 to 6 cycles prior to testing in order to allow it to reach a steady state in mechanical behavior. The setup was used to apply gradually increasing pressure reaching about 100 Pa, which is a pressure level much lower than the maximum pressure used in testing for the measurement of Young's modulus.

Step increases in pressure were applied from 0 to 1kPa inside the bulla with stopcock

closed for each step ensuring that a constant pressure was maintained. Both positive pressure (pumping air into bulla) and negative pressure (vacuuming air from bulla) were applied to the samples. The samples were applied positive middle-ear pressures in the order 0.2, 0.25, 0.3, 0.5, 0.6, 0.75, 0.8, and 1 kPa then released with reverse order to 0kPa. The TM was then vacuumed up with negative middle-ear pressures in the same order up to 1kPa and released with reverse order to 0kPa, which was considered as one cycle. For each sample, at least four cycles were tested and the average was used for analysis. The pressure values used in this experiment cover the pressure range normally encountered in daily life.

The fringe projection system consistently projected fringes pattern onto the guinea pig TM (figure 4.8 (b)) and recorded the images of normal state and images of under all the pressure states, storing with a PC. Preprocessing was applied for each image using the normalization algorithm and then wrapped phase maps of TM surfaces were obtained by using algorithm in chapter II. The reconstruction of all these surfaces was then achieved by unwrapping these wrapped phase maps with free demodulation software (Ean Pitterson, Experimental Mechanics website). The depth maps of TM sample obtained from fringe projection reconstruction were exported as matrices correspond to pixels in images (figure 4.8 (a)). The TM boundary and the malleus location were determined by observation of input image. The useless background information were cut-off and the useful data on TM were used to calculate the volume displacement by comparing the under-pressure state with initial state.

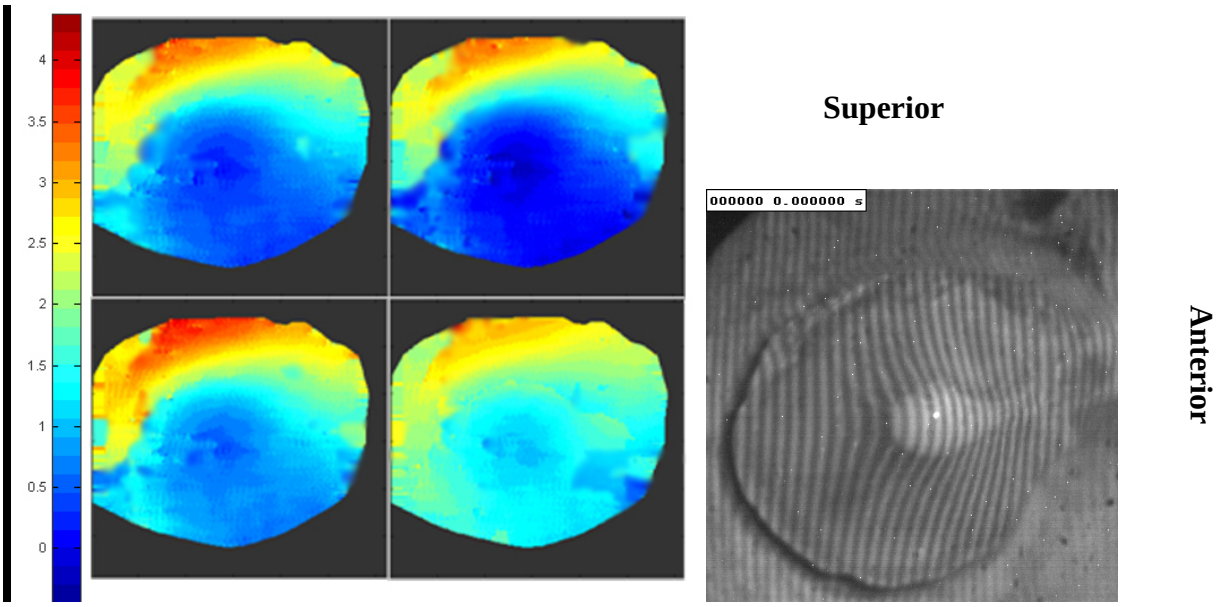

(a) (b)

Figure 4.8: (a) Reconstruction of TM surface. Started from right top in counter-clock wise, respectively is TM under pressure of 0kPa, 200Pa, 500Pa, and 1kPa. (b). TM under projected fringes correspond to the reconstructed surface.

CALCULATION OF VOLUME DISPLACEMENT

In order to obtain the full-field description of the TM's mechanical properties, pressure-volume displacement curve has to been extracted from the depth map as well as the

applied pressure history. Dirckx et al. presented a method to calculate the volume displacement in [32]. In this paper, a simpler way was used to obtain the volume displacement. We assume that each pixel in the reconstruction depth image represents a cuboid with depth different from normal case as high and pixel size as length. Thus the volume displacement can be simple calculated by the volume of all these cuboids.

Figure 4.9-4.10 shows the pressure-volume displacement curves of the 7 guinea pig samples, while figure 4.11 shows the average pressure volume displacement plot of all the 7 samples. The two graphs were separated by the date the sample received. From the figures, a clear hardening effect can be seen especially at high pressure above 500 Pa. Therefore, hyperelastic model should be used to describe the mechanical property of TM under high level pressure.

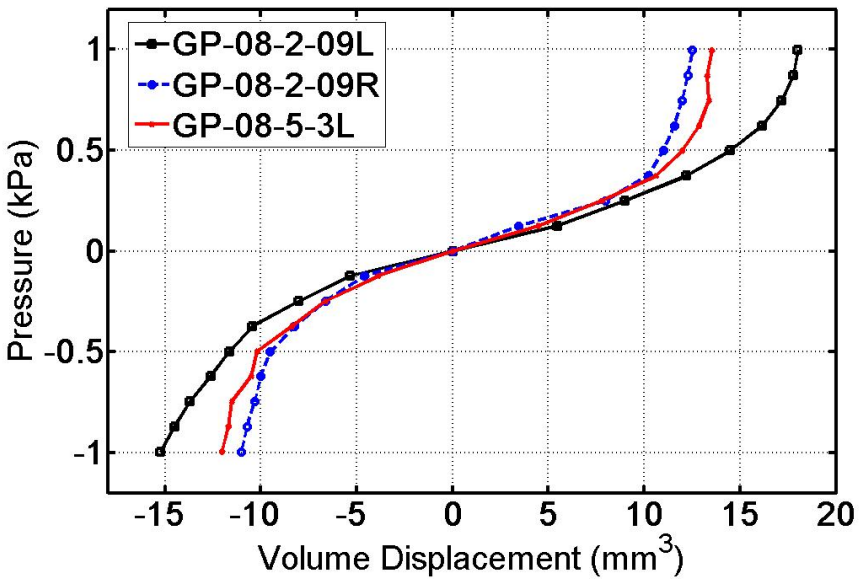

Figure 4.9: Typical Pressure-volume Displacement Plot of Guinea Pig TM.

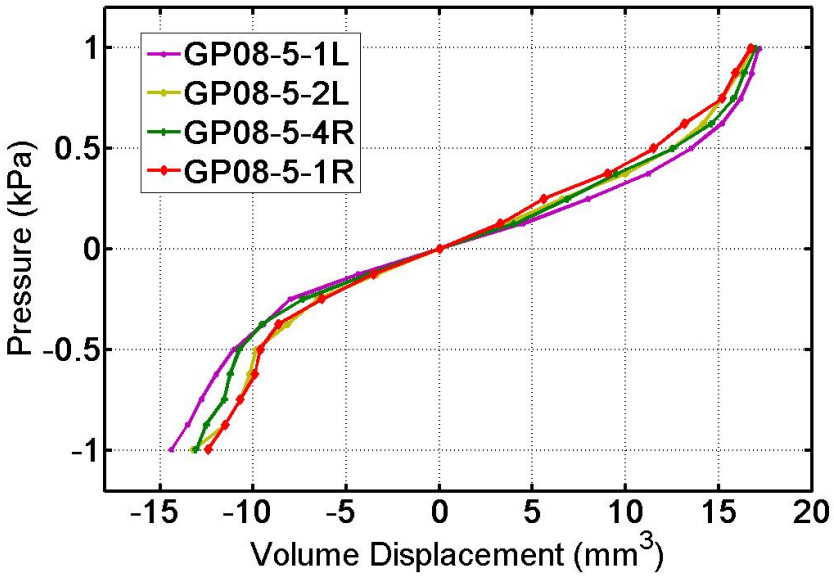

Figure 4.10: Typical Pressure-volume Displacement Plot of Guinea Pig TM.

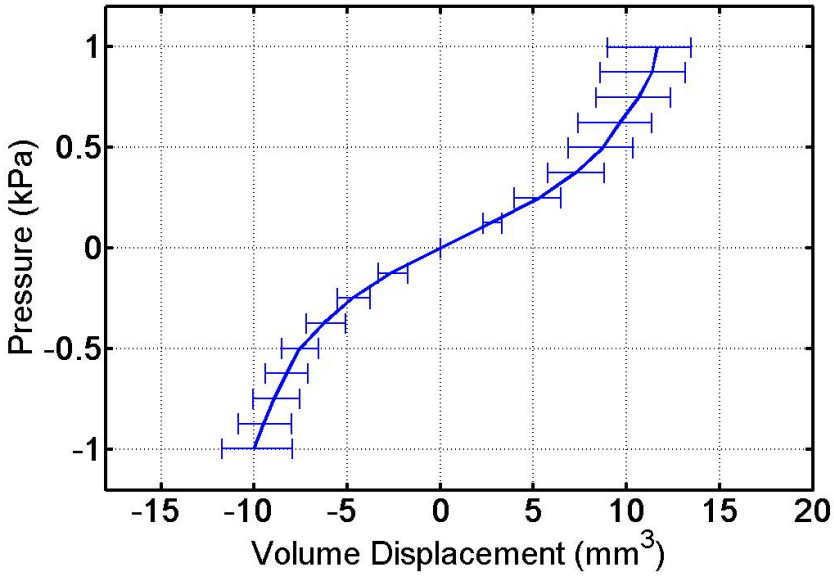

Figure 4.11: Average Pressure-volume Displacement Plot of 7 Guinea Pig TMs.

CHAPTER V

FINITE ELEMENT MODEL OF GUINEA PIG TYMPANIC MEMBRANE

INVERSE PROBLEM FOR ABSTRACTIN MECHANICAL PROPERTIES OF TM

Since trend of volume displacements versus pressures of TM shows hardening phenomenon, in order to analyze such hyperelastic effect, a classic hyperelastic model, Ogden model was used to describe the mechanical properties of TM. The constitute law of uniaxial mode of the Ogden model is as follows [33]:

$$\lambda_1 = \lambda_U, \lambda_2 = \lambda_3 = \lambda_U^{-\frac{1}{2}}, \qquad \lambda_U = 1 + \varepsilon_U$$

$$T_U = \sum_{i=1}^{N} \frac{2\mu_i}{\alpha_i} \left(\lambda_U^{\alpha_i - 1} - \lambda_U^{-\frac{1}{2}\alpha_i - 1}\right) \quad (i = 1, 2, \ldots N)$$

where ε_U is strain, T_U is stress, $\lambda_i \ (i = 1,2,3)$ are the principle stretch, μ_i and α_i are mechanical properties of hyperelastic material respectively. In our analysis, N was chosen as 2. In order to determine mechanical properties $\mu_i$and α_i an inverse problem solving approach is used by allowing the finite element method (FEM) simulated TM deformation data to correlate with the measured values. The procedure is described as follows:

1. Some initial values were chosen for μ_i and α_i .

2. A FEM Neo-Hookeon model was built as is shown in Figure 5.3. In order to compare with experimental data. The out-of-plane (the plane parallel to image plane of the camera) displacement of every node was obtained.
3. Displacement of nodes from 2 were interpolated to back ground gridding whose intercepting point density is the same as pixel density of images obtained in experiment. Bilinear interpolation was used to implement the process [34, 35].
4. Calculated volume displacement based on out of plane displacement of back ground gridding, using the same method that was used to calculate volume displacement from experimental data by assuming volume change of every pixel as cuboid.
5. Modified μ_i and α_i of 1 and repeated 2 to 4 until the volume displacement from simulation fit volume displacement from experimental data.

The simulation of the guinea pig TM under different air pressure states was implemented using Abaqus 6.8. The compacted FEM software is able to provide preprocessing of the modeling, FEM computation and post-processing for computational visualization and analysis. In this work, the output from the FEM computation in use is the z-direction displacement in that it is the counterpart to the available information obtained from fringe projection system. The step 3 and 4 are not accessible in Abaqus, thus the algorithm was program with Visual Basis 6.0 to calculate the volume displacement (figure 5.1). It should be note that, in order to save computational time, the corresponded pressure steps in the experiment was computed and analyzed simultaneously in one task, instead of simulating one pressure step in one task. Meanwhile, the volume displacement

calculation program was designed to handle the whole loading circle simultaneously (See appendix C).

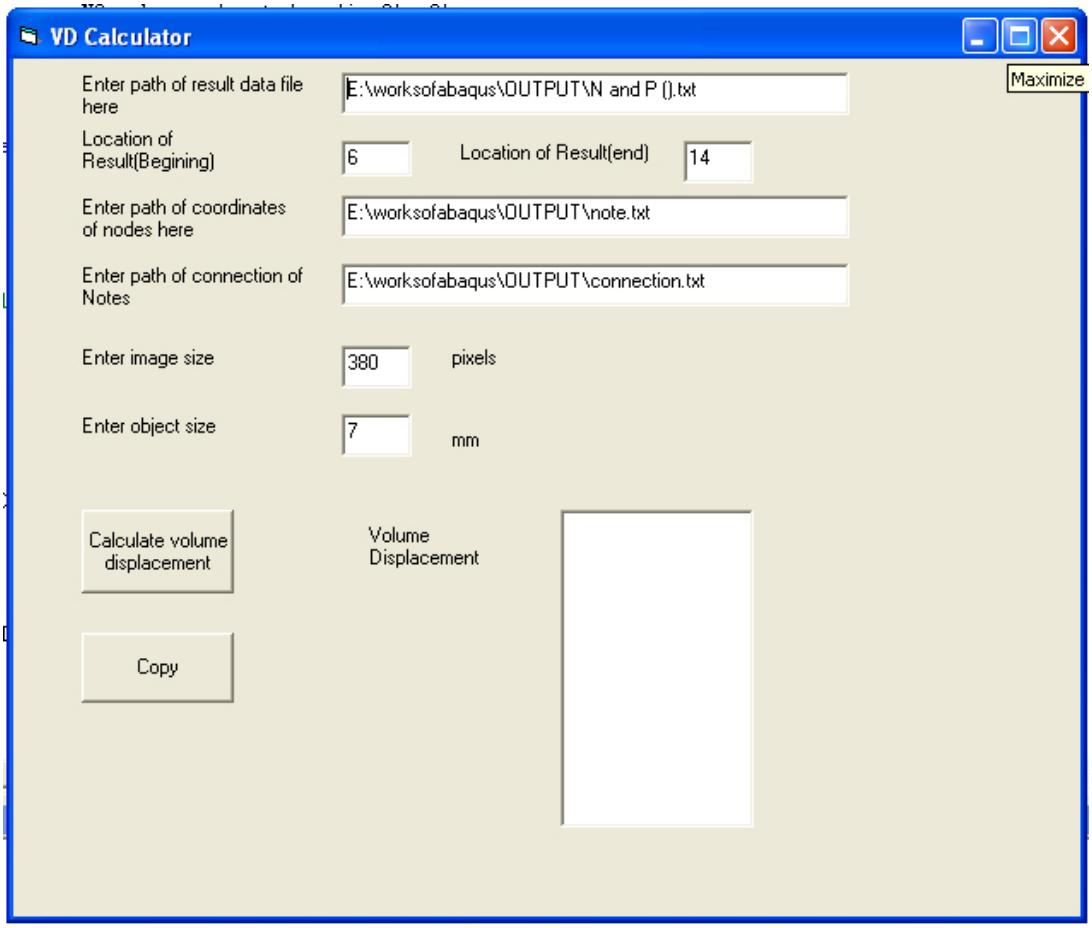

Figure 5.1: Interface of Program for Volume Displacement Calculation.

FINITE ELEMENT OF TM

A FEM model of guinea pig TM was needed for the estimation algorithm for the measurement of mechanical properties. In order to obtain the geometry of the FEM

model tailored to each particular guinea pig TM, reconstructed surface profiles of sample in initial state from fringe projection algorithm were used. However, the geometry information of guinea pig TM from the fringe projection algorithm was in form of matrix of depth map and such type of data was unable to be applied to FEM simulation. In order to transfer the matrix of depth map into the form of notes and elements in FEM computation, Solidworks 9.0, a CAD software was used to build the FEM model. 20 lines of data along the superior–inferior direction in the TM depth map were selected. The background data in these lines was setting to null number by comparing the corresponded locations in depth maps with that in the actual images. These null numbers were then removed and input as special curves to Solidworks (See appendix D). These curses then were lofted into the feature as an intact TM (figure 5.2). The 20 lines chosen were evenly distributed over the depth map--such simplification was required in that too many curves could induce interpolation error in generation of the FEM model. Since surface of guinea pig TM was smooth, evenly chosen data means smoothing of the surface, which will not compromise the reliability of the significantly.

Finally, the geometry of the model was modified at the edge so that a clear and regular boundary condition can be achieved. The location of the malleus in the FE model was determined by isolated malleus in the actual image of TM sample. An artificial malleus was “merged” into the TM by setting the contact area between malleus and TM as material with mechanical properties of bone. In order to analyze all of the samples with one FE model, the dimension of the model was modified in two directions based on Table 1 for each sample: Superior-inferior and Anterior-posterior.

The boundary conditions of the FE model were designed as to simulate the actual situation. The outer boundary of the TM was fixed for all degrees of freedom. The malleus was allowed to rotate and move out of z direction only. Although in actual case, malleus can function as a damping boundary condition, it was shown that there was not too much change for the movement of the soft tissue when changing the malleus boundary condition [36]. The mechanical property of malleus was set to be elastic with a Young's modulus of 10 GPa. Since the difference between soft tissue and malleus is huge, the precision of the number of that does not have too much affect to the displacement of soft tissue [37].

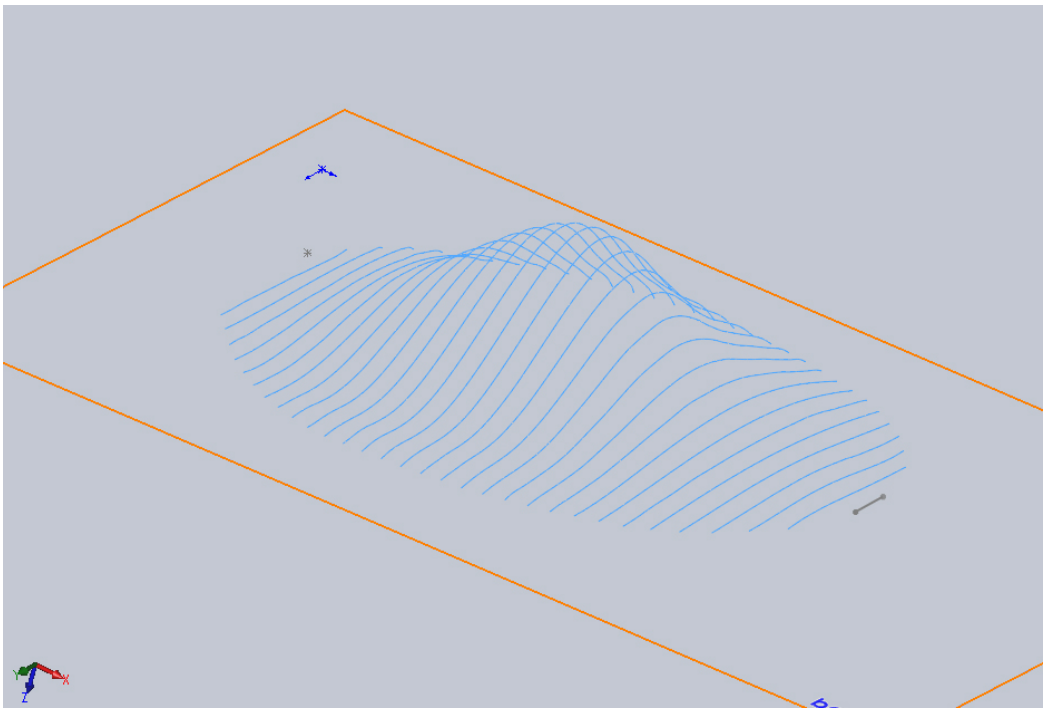

Figure 5.2: Extracted Curves for FEM Model Construction.

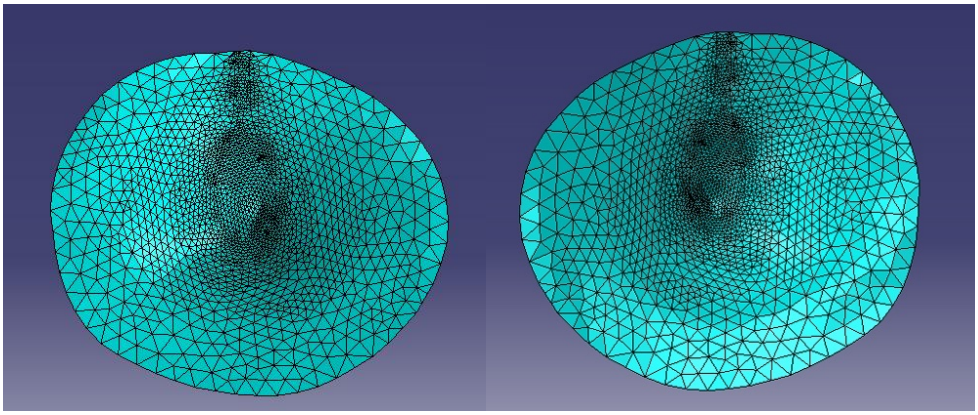

(a) (b)

Figure 5.3: FEM model of TM (a).Medial view (b). Lateral view.

CHAPTER VI

MECHANICAL PROPERTIES ANALYSIS OF TYMPANIC MEMBRANE

RECONSTRUCTION OF TM SURFACE UNDER PRESSURE

RESULTS OF HYPERELASTIC MEASUREMENT

Figure 6.1 shows the typical fitting of the pressure- volume displacement curve between FEM and experimental data. The curves were fitted with difference less than 10% between FEM and experimental data so that an accurate hyperelasticity was obtained. Figure 6.2 shows the hyperelastic properties of guinea pig TM respectively under positive middle ear pressure and negative middle ear pressure. The maximum of the strain in the plot is the maximum strain in the TM FEM model when 1 kPa pressure was applied. It can be seen that the corresponded Young's modulus of guinea pig TM is around 20MPa at maximum which is lower than human TM (0.02-0.04 GPa) and cat TM [12]. The hyperelastic parameters for the 7 samples were listed in Table 6.1 and Table 6.2 respectively under positive middle ear pressure and negative middle ear pressure.

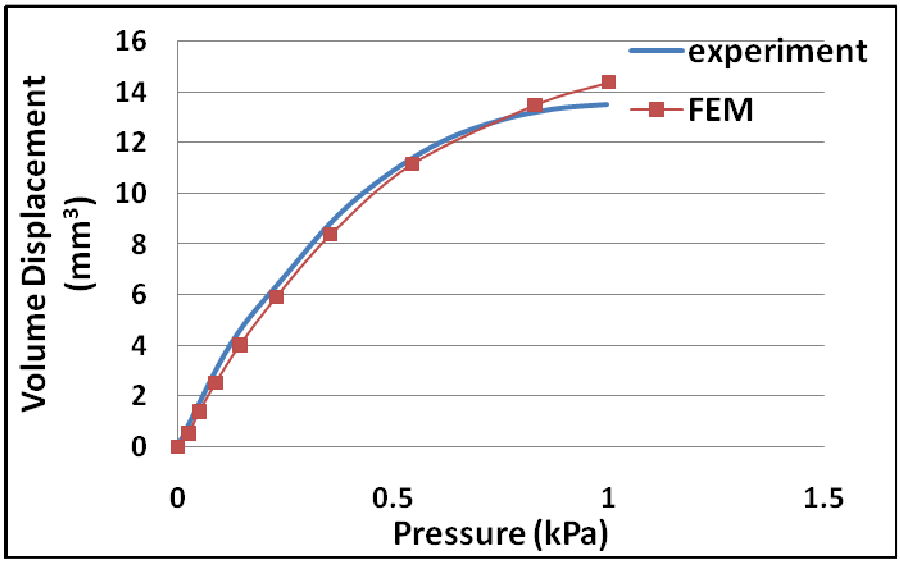

Figure 6.1: A typical fitting between FM and experimental data for guinea pig TM

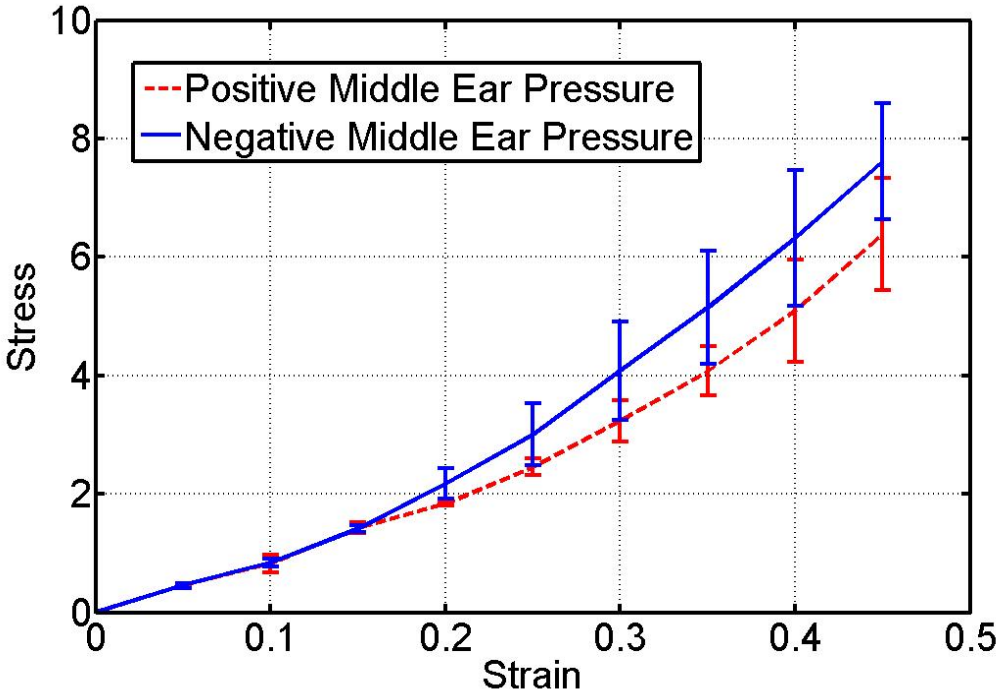

Figure 6.2: Hyperelasticity of Guinea Pig TM

Sample	Ear	μ1(MPa)	α1	μ2(MPa)	α2
GP-08-2-09	Right	0.48	9.82	8.92	-4.56
GP-08-2-09	Left	0.41	10.48	9.3	-5.01
GP-08-5-3L	Left	0.48	9.52	9.27	-4.31
GP-08-5-1L	Left	0.44	12.85	7.96	-5.62
GP-08-5-2L	Left	0.59	8.23	8.5	-4.67
GP-08-5-4R	Right	0.35	9.62	8.23	-4.33
GP-08-5-1R	Right	0.41	9.88	9.01	-5.32

Table 6.1: Hyperelastic Parameters of Guinea Pig TM under positive Middle Ear Pressure

Sample	Ear	μ1(MPa)	α1	μ2(MPa)	α2
GP-08-2-09	Right	0.61	9.06	9.17	-4.43
GP-08-2-09	Left	0.52	10.02	9.88	-5.21
GP-08-5-3L	Left	0.61	9.12	9.46	-4.43
GP-08-5-1L	Left	0.56	11.34	8.22	-5.45
GP-08-5-2L	Left	0.59	8.03	8.75	-4.88
GP-08-5-4R	Right	0.43	9.22	8.77	-4.54
GP-08-5-1R	Right	0.49	9.78	9.4	-5.47

Table 6.2: Hyperelastic Parameters of Guinea Pig TM under Negative Middle Ear Pressure

DISCUSSION AND CONCLUSION

(a). Deformation Analysis

In order to have a better understanding and clearer view of the deformation of guinea pig TM under different pressures and at different locations, cross section profile was plotted in two perpendicular directions: the superior-inferior direction and anterior-posterior direction. Figure 6.3 shows the cross section profile of TM under different pressure levels. It can be seen that in the superior-inferior cross section, the maximum displacements roughly occur at the center and the displacement gradually decrease to both anterior and posterior direction. Finally, the displacement reach zero at the boundary. This trend is similar in both anterior portion and posterior portion of the TM. Meanwhile, in case of anterior-posterior section, the displacement distribution differentiates dramatically from superior-inferior situation. The displacements are generally close to zero around the umbo and gradually increase to two maximum points: both are between the boundary and the umbo. In the radial direction, after passing these two maxima, the displacement gradually decreases to zero where the boundary is located. This is can be explained as that due to the connection between the malleus and TM, the stiffer properties of the malleus weaken the displacement of the TM. However, on the posterior side close to umbo, there is a sudden displacement increase. This indicate that the malleus under pressure more likely tend to rote rather than bend. The stiffness difference between TM and malleus was one reason while the asymmetric geometry of TM (TM area is larger in posterior than anterior) and malleus can also contribute to such

a rotation when pressure is applied.

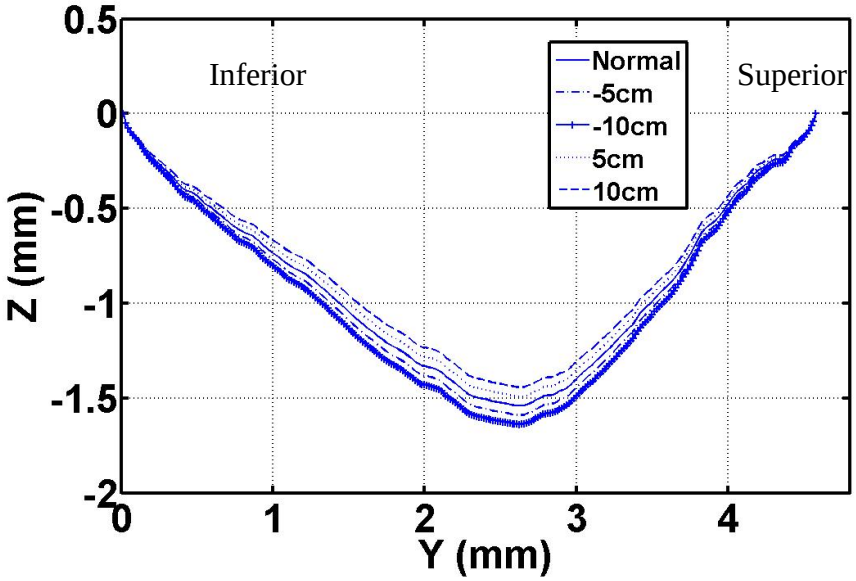

(a)

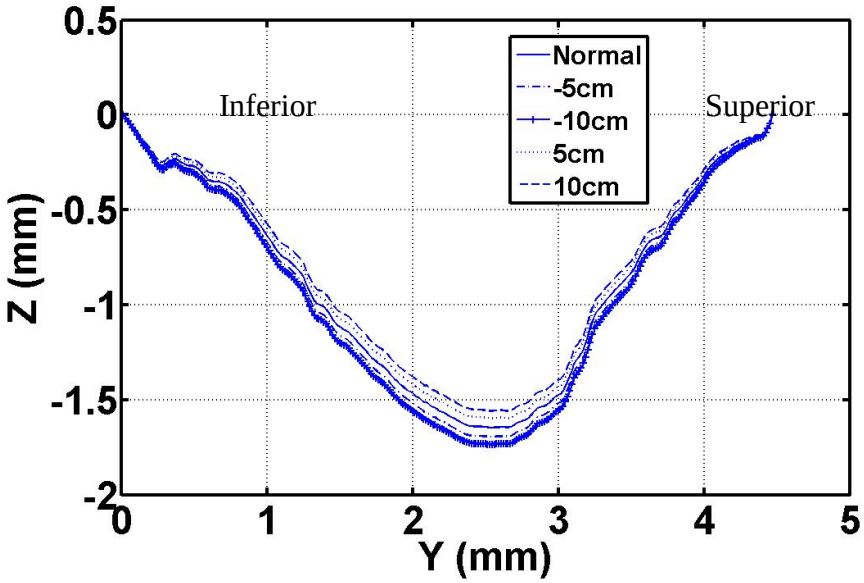

(b)

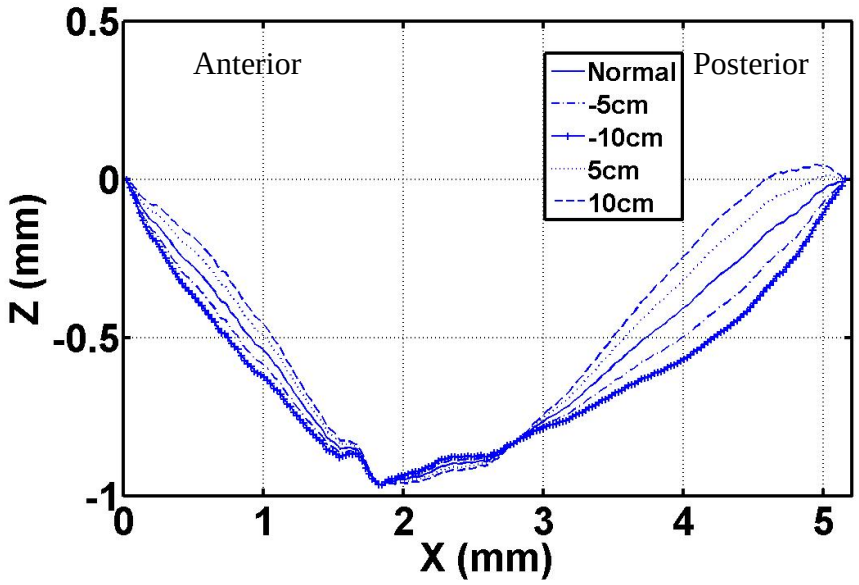

(c)

Figure 6.3: Pressurized shape for guinea pig TM. In the legend, the "cm" indicated pressure in unit of water bar.(a) Superior-interior cross section in anterior. (b) Superior-interior cross section in posterior.(c) Anterior-posterior cross section in posterior.

(b). Hardening Effect

The observed the pressure-volume displacement curves in figure 4.9-4.11 indicate that TM response is not elastic; the increase of response is non-linear by with a positive acceleration. Similar to rubber, TM becomes significant stiffer as loading increase, showing some extend of hardening effect. Therefore for quasi-static study of TM, hyperelastic model is better than elastic model. The hyperelastic property of TM under quasi-static loading can be further vilified through the mechanical properties estimated by the fitting experimental data with simulation data, shown in figure 6.2. Since sound impedance increase as the material stiffness increase, hyperelasticity of TM can affects

the efficiency of the function of middle ear. This can probably explain why the sudden increase of middle ear pressure in some situations-such as in a sudden rising elevator or in a taking off plane- can lead to a transient loss of hearing [39].

Comparison between the positive middle ear pressure and negative middle ear pressure results in figure 4.11 also shows that the hardening effect of TM is more significant under negative pressure then under positive pressure, *i. e* the TM becomes much stiffer if pressure level in ear canal is higher than middle ear. This phenomenon can be explained through the geometry of TM. TM is a concave to ear canal while convex to middle ear. When pressure level is higher in ear canal, it tends to "enlarge" the TM by stretching the circumferential collagen fibers. On the other hand, when pressure level is higher in middle ear cavity, the air force the TM to "shrink" releasing some tension and hence offset some hardening effect from material property. Last but not least, the radial collagen fibers can also play a role in damping the hardening effects by that they are originally bending toward ear canal with certain level of pre-stretch.

(c). Comparison with Literature

The Young's modulus obtained by fitting FEM data with experimental data in this work is full-field mechanical property but an "effective" Young's modulus; because the simulation was based on the assumption that TM consists of homogeneous, isotropic material and the thickness as well as mechanical property is uniform over the whole TM.

In actual case, thickness over TM varies from location to location [40][41], and hence the mechanical properties can also vary.

So far, there is not many Young's modulus measured on animal. The available data that can be found are on rabbit about 30MPa [42] and some estimation data on cat about 0.1-0.4 GPa[12]. For human TM, Young's modules are reported in different situations. Von Bekesy presented a data about 20MPa using the assumption of isotropy, so his estimate is also an effective one [10]. Kirikae and Decraemer et al. estimate the Young's modulus of human TM to be 40 MPa and 23 MPa, respectively [9,11]. Both involved uniaxial tensile testing of strips cut from the TM. Our results show that the Young's modulus of Guinea pig TM is about 13.4- 18.2 MPa which is a bit lower than the above existing data but in the same magnitude. Such difference can be generated from the differences in species. Hence, in further work the same technique can be applied to human TM to determine if our technique produces the same effective Young's modulus for the human TM.

Recent studies, indicated strong rate-dependence for organs such as ligaments, skin, muscle, stomach, liver, heart and lung at high strain rates (>10 s^{-1}) [3]. However not many investigations were made on such phenomenon in animal TM, especially in full-field observation. In this work, we have not only shown that rate-dependence happen on animal TM, but also presented the hyper-elastic properties of animal TM. The full-field measurement indicates a hardening effect of guinea pig TM i.e. Young's modulus increase as strained rate increase.

(d). Hysteresis of Experimental Result

Figure 6.4 shows a typical guinea pig TM (GP-8-51L) under loading and unloading air pressure with the same experimental procedure discussed in Chapter IV except that the releasing steps was also included. The original shape of the TM was not restored when loads were removed. Such hysteresis effect indicates that guinea pig TM like many other tissues, is viscoelastic. Therefore it is better to model the TM as viscoelastic material than hyperelastic material if time-dependent phenomenon is considered. However, for viscoelastic testing, it usually requires a long time loading and unloading process. On the other hand, for full-field mechanical testing, the maintenance of the intact bulla demands that cadaver TM should not be exposed to the air for a long time; otherwise the TM will dehydrate or even damaged. Even if creep loading is not required, there is still difficulty to accurately measure the loading time- unlike other loading pressure delay always exists. Therefore, the full-field measurement of viscoelasticity of TM remains a unsolved challenge and is left to future work.

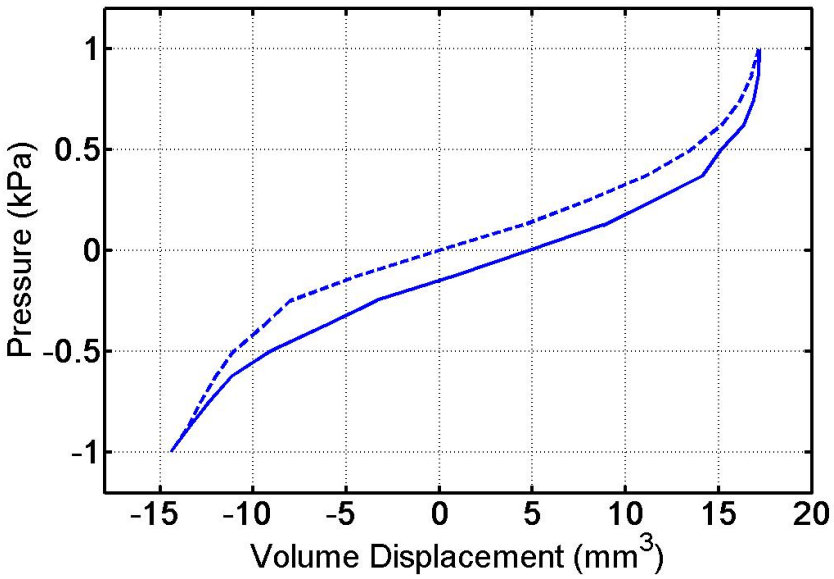

Figure 6.4: Loading and Unloading Plot for Static Pressure Test

CONCLUSION

Full-field mechanical properties of guinea pig TM was achieved by fitting experimental data with simulation results. Fringe projection technique was first introduced to research of TM. Although projection moiré has been used for observation of TM deformation, the fringe projection surpasses projection moiré in convenience of setup and reliability on calibration without satisfying the resolution. The TM was modeled as hyperelastic material instead of elastic material so that hardening effect is revealed. Although using viscoelastic model can more suitably depict the hysteresis phenomenon of TM under loading-unloading cycle, some unsolved difficulty hinders the viscoelastic analysis. Consider that hyperelastic model already can satisfy the requirement of quasi-static loads, the full-field viscoelasticity study of TM will be future work. FEM model was built with

combined fringe projection reconstruction and CAD soft ware. Compare to traditional FEM model built with CT scan or artificial middle ear model, the model in this work are more detail and able to use for real-time measurement.

Section profile of the TM deformation under different pressure loading was observed with fringe projection reconstruction. It was found that due to asymmetric geometry of TM and malleus itself, the malleus under high pressure is more likely to rotate than to translate. Hyperelasticity of guinea TM under positive middle ear pressure and negative middle ear pressure was compared. It shows that hardening effect of TM is more significant when it under high canal ear pressure than high middle ear pressure, which can due to two factors: the concave geometry of TM and the collagen fiber alignment in its grid work. The estimated moduli were obtained in range from 13.4- 18.2 MPa. Comparing to the existed data in literature, they are in the same magnitude.

Since middle ear structure of guinea pig is almost identical that of human, the research on guinea pig TM sheds light on the further human middle ear research. In the future, attempt can be move on to miniaturized fringe projection system in single apparatus, based on which, *in vivo* measurement mechanical properties of TM will be achievable. Meanwhile, although dynamic test in frequency range is not able to implement with pressure loading, there is still significance in observing TM encounter ultra-high pressure until it bursts. High- speed camera can be induced in this kind of study. The only difficulty is from the sensitivity of pressure measurement in high speed. Other loading can also be attempted to estimate the viscoelasticity of TM, for example, indentation on

TM can also provide full-field measurement of mechanical properties, and and this technique has never been used for viscoelasticity test yet [43].

REFERENCES

[1]. G. H. A. Cole, “International Series of Monographs on Physics-The Physics of the Ear”, Vol. 3, Pergmamon Press, 1965.

[2]. Stanley A. Gelfand, “Hearing- An Introduction to Psychological and Physiological Acoustics,” Marcel Dekker, Inc., 1981.

[3]. Lu, H., Luo, H. and Gan, R. “Measurements of Young’s Modulus of Human Eardrum at High Strain Rates Using a Miniature Split Hopkinson Tension Bar”, *Proc.* 2007 SEM Ann. Conf., Vol. 1, pp.190–194, 2007.

[4]. William A. Yost, “Fundamentals of Hearing-An Introduction,” 2nd ed. Elsevier Inc., 2007.

[5]. Richard D. Rabbitt, Mark H. Holmes, “A Fibrous Dynamic Continuum Model of the Tympanic Membrane”, J. Acoust. Soc. Am., Vol. 6, pp. 1716-1728, 1986.

[6]. Joris J.J. Dirckx and Willem F. Decraemer, “Human Tympanic Membrane Deformation under Static Pressure”, Hear Rs, Vol. 51, pp.93-106, 1991.

[7]. Gang Huang, Nitin P. Daphalapurkar, Rong Z. Gan, and Hongbing Lu, “A Method for Measuring Linearly Viscoelastic Properties of Human Tympanic Membrane Using Nanoindentation”, Journal of Biomechanical Engineering, Vol.130, pp. 1-7, 2008.

[8]. Nitin P. Daphalapurka, Chenkai Dai, Rong Z. Gan, Hongbing Lu, “Characterization of the Linearly Viscoelastic Behavior of Human Tympanic Membrane by Nanoindentation”, Journal of the mechanical behavior of biomedical materials, 2009, Vol.2, pp. 82-92, 2008.

[9]. I. Kirikae, “The Structure and Function of the Middle Ear”, University of Tokyo Press, Tokyo, 1960.

[10]. G. Von Bekesy, “Experiments in Hearing”. McGraw Hill, New York, 1960.

[11]. W.F. Decraemer, M. A. Maes, V. J. Vanhuyse, “Analytic Stress-strain Relation for Soft Biological Tissues Based on a Structural Model”. J. Biomech., Vol.13 pp.463-468, 1980.

[12]. Jonathan Fay, Sunil Puria, Willem F. Decraemer, Charles Steele, “Three Approaches For Estimating the Elastic Modulus of the Tympanic Membrane”, Journal of Biomechanics, Vol.38, pp.1807–1815, 2005.

[13]. Anil K. Jain, Mário Figueiredo, and Josiane Zerubia, “Energy Minimization Methods in Computer Vision and Pattern Recognition”, Springer Press, 2001.

[14]. M. Heredia, “Novel Developments of Moiré Techniques for Industrial Applications”, Doctoral Thesis, Sheffield, UK, university of Sheffield, 2004.

[15]. Daniel Malacara, Manuel Servin, and Zacarias Malacara, “Interferogram Analysis for Optical Testing”, Marcel Dekker Press, 1998.

[16]. D. C. Ghiglia, and M. D. Pritt, “Two-dimensional Phase Unwrapping”, John Wiley and Sons, New York, 1998.

[17]. Tao Cheng, Chenkai Dai, Rong Z. Gan, “Viscoelastic properties of human tympanic membrane”, Annals of Biomedical Engineering, Vol. 35, No. 2, pp. 305-314, 2007.

[18]. Luo, H., Dai, C., Gan, R. and Lu, H. “Measurement of Young’s modulus of human tympanic membrane at high strain rates”, J. Biomech Eng. – Trans ASME, submitted 2008.

[19]. Flisberg K., Ingelstedt S. and Ortegren U., “On Middle Ear Pressure”, Acta Otolaryngol(Stokh.). Suppl, Vol. 182, pp. 43-56, 1963.

[20]. Elner A., Ingelstedt S. and Ivarsson A., “The Elastic Properties of the Tympanic Membrane System”, Otolaryngol (Stokh.), Vol.72, pp. 397-403, 1971.

[21]. M.von Unge, W.F Decraemer, D. Bagger-Sjoback, J. J. Dirckx, “Displacement of the Gerbil Tympanic Membrane under Static Pressure Variations Measured with a Real-

time Differential Moiré Interometer", Hearing Research, Vol. 80, No.2, pp.229-242, 1993.

[22]. M. von Unge, W. F, J.J. Dirckx, D. Bagger-Sjoback, "Shape and Displacement Patterns of the Gerbil Tympanic Membrane in Experimental Otitis Media with Effusion", Hearing Res, Vol. 82, pp. 184-196,1994.

[23]. Hanif M. Ladak, Willem F. Decraemer, Joris J.J. Dirckx, and W.Robert J. Funnell, "Respose of the Cat Eardrum to Static Pressures: Mobile Versus Immobile Malleus, J.Acoust". Soc. AM, Vol. 5, pp. 3308-3021, 2004.

[24]. Michael Gaihede, Donghua Liao, and Hans Gregersen, "In Vivo Areal Modulus of Elasticity Estimation of the Human Tympanic Membrane System: Modeling of Middle Ear Mechanical Function in Normal Young and Aged Ears", Phys Med Biol, Vol.52, pp.803-814, 2007.

[25]. Lisa L. Hunter and Robert H. Margolis, "Effects of Tympanic Membrane Abnormalities on Auditory Function", J Am Acad Audiol, Vol.8, pp.431-446, 1997.

[26]. Susan E. Voss, Johne J. Rosowski, Saumil N. Merchant, William T. Peake, "Acoustic responses of the Human Middle Ear", Hearing Res, Vol. 150, pp.43-69, 2000.

[27]. Rong Z. Gan, Mark W. Wood, and Kenneth J. Dormer, “Human Middle Ear Transfer Function Measured by Double Laser Interferometry System”, Otology & Neurotology, Vol.25, pp.423-435, 2004.

[28]. Mehmet F.Oktay, Sebahattin Cureoglu, Patricia A. Schachern, Michael M. Paparella, Shin Kariya, Hisaki Fukushima, “Tympanic Membrane Changes in Central Tympanic Membrane Perforations”, American Journal of Otolaryngology-Head and Neck Medicine and Surgery, Vol.26, pp.393-397, 2005.

[29]. J.A.N. Buytaert, J. E. F Aernouts, J.J.J. Dirckx, “Indentation Measurements On the Eardrum with Aautomated Projection Moiré Profilometry”, Optics and Lasers in Engineering, Vol 47, pp301-309., 2009.

[30]. M. Heredia Ortiz and E. A. Patterson “On the Industrial Applications of Moiré and Fringe Projection Techniques”, Strain, Vol. 39, pp. 95-100, 2003.

[31]. M. Heredia Ortiz and E. A. Patterson, “Location and Shape Measurement Using a Portable Fringe Projection System”, Society for Experimental Mechanics, Vol.45, 2005.

[32]. J.J.J Dirckx, W. F. Decraemer, M. von Unge, Ch. Larsson.” Volume Displacement of the Gerbil Eardrum Pars Flassicda as a Function of Middle Ear Pressure”, Hearing Res, Vol.118, pp.35-46, 1998.

[33]. “ Hyperelastic Material Behavior”, Abaqus Theory Manual 6.7.

[34]. S. G. Bardenhagen and E.M. Kober, “The Generalized Interpolation Material Point Method”, CMES, Vol.5, pp.477-495, 2004.

[35]. Rafael C. Gonzalez and Richard E. Woods, “Digital Image Processing”, 2nd ed, Publishing House of Electronic Industry, Beijing.

[36]. Tuchk-Lee, J.P., P.M., Steele, C.R., Puria, S.,” Finite element modeling of acoustomechanical coupling in the cat middle ear”, J. Acoust. Soc. Am, Vol.124, pp.348-362, 2008.

[37]. Ladak, H.M., Funnell, W.R.J, Decraemer, W.F, Dirckx, J. J.J, “ A Geometrically Nonlinear Finite-Element Model of the Cat Eardrum”. J. Acoust. Soc. Am, Vol.119, 2859-2868.

[38]. Jacob Sade, “The Buffering Effect of Middle Ear Negative Pressure by Retraction of the Pars Tensa”, the American Journal of Otology, Vol.21, pp.20-23, 2000.

[39]. Hergils L. and Magnuson B.,”Morning Pressure in the Middle Ear”, Arch. Otolaryngol, Vol.111, pp.86-89.

[40]. L.C. Kuypers, J.J.Dirckx, W.F. Decraemer, “Thickness measurements of a cat’s eardrum by use of a confocal microscop”, Association for Research in Oto-Laryngology Abstracts, 2001.

[41]. L.C. Kuypers, J.J.Dirckx, W.F. Decraemer, “Thickness distribution of a human eardrum measured with confocal microscope”, Association for Research in Oto-Laryngology Abstracts, 2003.

[42]. J. E. F. Aernouts, J. A. M. Soons, J.J.J. Dirckx, “Quantification of Tympanic Membrane Elasticity Parameters from *in situ* Measurements”, MEMRO 2009 5th International Symposium, Stanford University, California, U.S.A.

[43]. Hesabgar, S.M., Ladak, H. M., Samani, A., Agrawal , S.K., “Measuring the Quasi-static Young’s modulus of the Eardrum Using Indentation Technique, MEMRO, 2009, 5th, International Symposium, Stanford University, California, U. S. A.

[44]. J. Tan, RA Tange, WA Dreschler, A Kleij, EC Tromp, “Long-term Effect of Hyperbaric Oxygenation Treatment on Chronic Distressing Tinnitus”.Vol.28, pp.91-106,1999.

APPENDICES

APPENDIX A

DAFT OF CUSTOM-MADE TEMPORAL BONE FOR GUINEA PIG

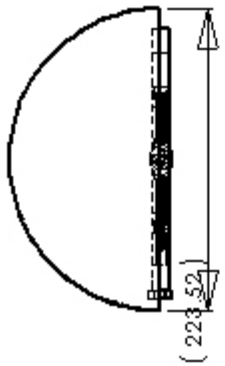

All the srews are 1/4-20.

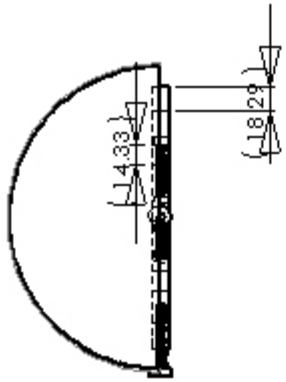

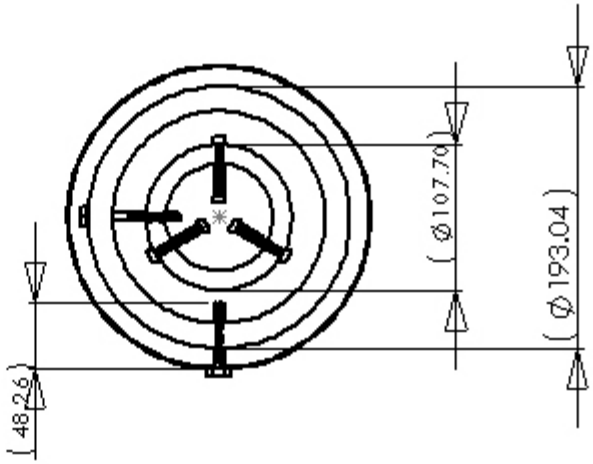

MATERIAL: ALUMINUM
FINISH: N/A
DESIGNER: JUNFENG LIANG
SCALE: 1=1

APPENDIX B

COMPUTER PROGRAM FOR NORMALIZATION FOR FRINGE PROJECTION PREPROCESSING

```
%%%%%%%%%%%%%%%%%%%%%%
%Normalization for background illumination%
%%%%%%%%%%%%%%%%%%%%%%

%Step 1. Divide image into blocks.
[M,N]=size(I);
m=min([1.5*P,M/60,N/60])
m=max(P+1,m);
n=min([1.5*P,M/60,N/60]);
num=fix(N/m);

%%
%Step 2. Estimation the background term.
for i=1:num
   A(i)=mean(I(m*i-9:m*i));
end
A(num+1)=mean(I(m*num+1:end));
p=polyfit([m/2+0.5:m:num*m-m/2+0.5,mod(N,m)/2+0.5+num*m],A,3);
f=polyval(p,1:N);
plot([m/2+0.5:m:num*m-m/2+0.5,mod(N,m)/2+0.5+num*m],A);
hold;
plot(f,'r');
fA=polyval(p,1:N);
```

```
%%
%Step 3. Estimation the modulation term.
for i=1:num
   tmp=A(i);
   B(i)=max(I(m*i-9:m*i)-tmp)-min(I(m*i-9:m*i)-tmp);
end
B(num+1)=max(I(m*num+1:end)-A(num+1))-min(I(m*num+1:end)-A(num+1));
p=polyfit([m/2+0.5:m:num*m-m/2+0.5,mod(N,m)/2+0.5+num*m],B,3);
fB=polyval(p,1:N);
%%
%Step 4. Removing the two terms.
NI=(I-fA)./fB;
%%
%Step 5. Re-scale the normalized image.
if min(NI)<0
   NI=NI-min(NI);
end
%%
%Smooth the image
h=[1,1,1];
h=h/3;
J=conv(NI,h)
```

APPENDIX C

VB PROGRAM FOR CALCULATION OF VOLUME DISPLACEMENT

```
Private Sub cmdCopy_Click()

With Clipboard

End With

Dim buf As String

Dim i As Long

For i = 0 To List1.ListCount - 1

    buf = buf + List1.List(i)

    buf = buf + vbCrLf

Next

Clipboard.Clear

Clipboard.SetText buf

End Sub


Private Sub Command1_Click()

List1.Clear

    Dim data(), note() As Double


''''''''''''''''''''''''''''''''''''''''

'Read results from Abagus output'

'                                    '

  Dim s() As String, j As Long, temp(), tmp2(), tmp4() As String

  Dim LocRe As Integer

  Dim ss() As String
```

```
Open Text1.Text For Input As #1
s = Split(StrConv(InputB(LOF(1), 1), vbUnicode), vbCrLf)
Close #1

tmp1 = Split(s(3), " ")
Dim k As Integer
k = 1
b = UBound(tmp1)
For i = 0 To UBound(tmp1)

   If tmp1(i) = "N:" Then
      ReDim Preserve tmp2(k)
      tmp2(k) = tmp1(i + 1)
      k = k + 1
   End If



Next

locB = Text6.Text
locE = Text8.Text
```

```
For LocRe = locB To locE


    tmp3 = Split(s(LocRe), " ")


    k = 1
    For i = 17 To UBound(tmp3)


        If tmp3(i) <> "" Then
            ReDim Preserve tmp4(k)
            tmp4(k) = tmp3(i)
            k = k + 1
        End If


    Next


''''''''''''''''''''''''''''''''''''''
'Read connections from Abagus output'
'                                    '
    Open Text2.Text For Input As #1
    ss = Split(StrConv(InputB(LOF(1), 1), vbUnicode), vbCrLf)
```

```
Close #1

ReDim note(UBound(ss), 4)
For i = 0 To UBound(ss) - 1

    temp5 = Split(ss(i), ",")

    For j = 0 To 3

       note(i + 1, j) = CDbl(Trim(temp5(j)))

   Next

Next

For i = 0 To UBound(note, 1)
   note(i, 3) = 0
Next

For i = 1 To k - 1

  note(tmp2(i), 3) = tmp4(i)
```

```
    Next

    Open Text7.Text For Input As #1
    ss = Split(StrConv(InputB(LOF(1), 1), vbUnicode), vbCrLf)
    Close #1

    ReDim con(UBound(ss), 4)
    For i = 0 To UBound(ss) - 1

        temp6 = Split(ss(i), ",")

        For j = 0 To 3

           con(i + 1, j) = CDbl(Trim(temp6(j)))

        Next

    Next

''''''''''''''''''''''''''''
'Traslate from node to pixels'
'                          '
''''''''''''''''''''''''''''
```

```
'Find points inside elements
"Limit searching area
  Const n = 380

   l = Text5.Text
   r = Round(l / n, 6)
   Dim Pixel(n, n) As Double

   For i = 1 To n

      For j = 1 To n

         Pixel(i, j) = 0
      Next

   Next
   For i = 1 To UBound(con, 1)
      Maxx = note(con(i, 1), 1)
      minx = note(con(i, 1), 1)
      Maxy = note(con(i, 1), 2)
      miny = note(con(i, 1), 2)
      For j = 2 To 3
         If note(con(i, j), 1) > Maxx Then Maxx = note(con(i, j), 1)
```

```
    If note(con(i, j), 1) < minx Then minx = note(con(i, j), 1)
    If note(con(i, j), 2) > Maxy Then Maxy = note(con(i, j), 2)
    If note(con(i, j), 2) < miny Then miny = note(con(i, j), 2)
 Next
For j = Int(minx / r) - 1 To Int(Maxx / r)
    For k = Int(miny / r) - 1 To Int(Maxy / r)
    'Interpolation for pixels inside elements
       X1 = note(con(i, 1), 1)
       X2 = note(con(i, 2), 1)
       X3 = note(con(i, 3), 1)
       Xp = j * r
       Y1 = note(con(i, 1), 2)
       Y2 = note(con(i, 2), 2)
       Y3 = note(con(i, 3), 2)
       Yp = k * r

       s1 = Abs((Xp - X3) * (Y2 - Y3) - (Yp - Y3) * (X2 - X3))
       S2 = Abs((X1 - X3) * (Yp - Y3) - (Y1 - Y3) * (Xp - X3))
       S3 = Abs((X1 - Xp) * (Y2 - Yp) - (Y1 - Yp) * (X2 - Xp))
       St = Abs((X1 - X3) * (Y2 - Y3) - (Y1 - Y3) * (X2 - X3))

    'If Round(St, 7) = Round(S1 + S2 + S3, 7) Then
```

```
                If St <= s1 + S2 + S3 Then
                    N1 = 1 - j * r / note(con(i, 2), 1) - k * r * (note(con(i, 2), 1) - note(con(i, 3),
1)) / note(con(i, 2), 1) / note(con(i, 3), 2)
                    N2 = (-k * r * note(con(i, 3), 1) + j * r * note(con(i, 3), 2)) / note(con(i, 2), 1)
/ note(con(i, 3), 2)
                    N3 = k * r / note(con(i, 3), 2)
                    nn = N1 + N2 + N3
                    Pixel(j, k) = N1 * note(con(i, 1), 3) + N2 * note(con(i, 2), 3) + N3 *
note(con(i, 3), 3)

                End If

            Next
        Next
    Next

''''''''''''''''''''''''''''''''
'Calculate Volume Displacement'
'                             '
''''''''''''''''''''''''''''''''
    VD = 0

    For i = 1 To n
```

```
        For j = 1 To n

            VD = VD + Pixel(i, j) * r ^ 2

        Next

    Next

    List1.AddItem VD

Next LocRe

Open "Output.txt" For Output As #1

For i = 0 To (locE - locB + 1)

 Print #1, List1.List(i)
' Print #1, vbCrLf


Next i
```

```
Close #1


End Sub
```

APPENDIX D

PROGRAM FOR FEM MODEL CONSTRUCTION IN SOLIDWORKS9.0 MICRO

```
'**********************
'This is the main program
**********************
Dim swApp As Object
Dim Part As Object
Dim SelMgr As Object
Dim boolstatus As Boolean
Dim longstatus As Long, longwarnings As Long
Dim Feature As Object
Sub main()

UserForm.Show
End Sub
```

```
*****************************
*This is the program in the button  *
*****************************

Private Sub CommandButton1_Click()

'Define some values
```

```
Dim n As Long
n = 10
m = 380 / n + 1
r = 7 / (m - 1)
Dim data() As Double
Dim border() As Integer
Dim s() As String, i As Long, j As Long, temp() As String
Dim SkN As String
Dim flag As Integer

'Import the data file
Open "C:\Documents and Settings\junfenl\My Documents\New Folder\test.txt" For Input
As #1
s = Split(StrConv(InputB(LOF(1), 1), vbUnicode), vbCrLf)
Close #1
ReDim data(m, m)
ReDim border(2, m)
For i = 1 To m
   temp = Split(s(i - 1))
   For j = 1 To m
      data(i, j) = CDbl(temp(j - 1))
   Next
Next
```

```
'Compress the data size
'For i = 1 To m
'    For j = 1 To m
'        data(i, j) = dataT((n / m) * i - (n / m) + 1, (n / m) * j - (n / m) + 1)
'    Next
'Next


'Find the object
For i = 1 To m
    j = 1
    flag = 0
    Do While (j <= m And flag < 2)
        If data(i, j) <> 0 And flag = 0 Then
            flag = 1
            border(1, i) = j
        End If
        If data(i, j) = 0 And flag = 1 Then
            flag = 2
            border(2, i) = j
        End If
        j = j + 1
    Loop
```

```
Next


'Solidwork anouncements
Set swApp = Application.SldWorks
Set Part = swApp.ActiveDoc
Set SelMgr = Part.SelectionManager
swApp.ActiveDoc.ActiveView.FrameState = 1


'Plot Lines
For i = 1 To m
    Part.InsertCurveFileBegin
    For j = border(1, i) To border(2, i) - 1
        Part.InsertCurveFilePoint (i - 1) * r, (j - 1) * r, data(i, j)
    Next
    Part.InsertCurveFileEnd
Next


'Contour the surface
For i = 1 To m
    SkN = Trim("Curve") + Trim(i)
    boolstatus = Part.Extension.SelectByID2(SkN, "REFERENCECURVES", (i - 1) * r,
border(1, i), data(i, 1), True, 0, Nothing, 0)
Next
```

```
Part.ClearSelection2 True
boolstatus = Part.Extension.SelectByID2("Curve1", "REFERENCECURVES", 0, 0,
data(1, 1), False, 1, Nothing, 0)
For i = 2 To m
   SkN = Trim("Curve") + Trim(i)
   boolstatus = Part.Extension.SelectByID2(SkN, "REFERENCECURVES", (i - 1) * r,
border(1, i), data(i, 1), True, 1, Nothing, 0)
Next

Part.InsertLoftRefSurface2 False, True, False, 1, 6, 6



End Sub

Private Sub UserForm_Click()

End Sub
```

VITA

Junfeng Liang

Candidate for the Degree of

Master of Science

Thesis: DETERMINATION OF THE MECHANICAL PROPERTIES OFGUINEA PIG TYMPANIC MEMBRANE USING COMBINED FRINGE PROJECTION AND SIMULATION

Major Field: Mechanical Engineering

Biographical:

Personal Data: Born in Guangzhou, Guangdong, China, May, 5, 1983, the son of Yueqiang Liang and Yunxian Zhang

Education: Graduated from the NO. 6 High School in Guangzhou in 2002; received Bachelor of Theoretical Mechanics degree from Jilin University, Changchun, China; complete requirements for the Master of Science degree from Oklahoma State University, with major in Mechanical Engineering , in July, 24, 2009.

Experience: Worked as a research assistant at Oklahoma State University from August, 2006, through July, 2009, principally on measurement of mechanical properties of guinea pig tympanic membrane; worked as a teaching assistant at Oklahoma State University from August, 2008, through December, 2008.

Professional Memberships: None

ADVISER'S APPROVAL: Hongbing Lu

Name: Junfeng Liang Date of Degree: December, 2009

Institution: Oklahoma State University Location: Stillwater, Oklahoma

Title of Study: DETERMINATION OF THE MECHANICAL PROPERTIES OFGUINEA PIG TYMPANIC MEMBRANE USING COMBINED FRINGE PROJECTION AND SIMULATION

Pages in Study: 97 Candidate for the Degree of Master of Science/Arts

Major Field: Mechanical Engineering

Scope and Method of Study: Measurement of the mechanical properties of guinea pig tympanic membrane (TM) with fringe projection and simulation. Fringe projection technique was used to provide optic access for measurement of the volume displacement of TM under different pressure levels. FEM model with hyperelastic constitute law was built to simulate the experimental procedure. Experimental data and simulation result were fitted to obtain the hyperelastic parameters of guinea pig TM.

Findings and Conclusions: Hardening effects was observed through pressure- volume displacement curve. The stress- strain curve plotted based on the estimated mechanical properties was also reflect such phenomenon. Comparison between the positive and negative pressure loading from middle ear cavity indicate that, such hardening effect is stronger as negative pressure applied.

The observation of the section profile of 3-D surface reconstruction of TM with Fringe projection technique shows that, the displacement around umbo is asymmetric. It means that the malleus tend to rotate rather than translate at high pressure level.

The experimental design was compared with other research group. Full-field mechanical properties measured with the designed experiment were validated by comparison to existed data in literature.

ADVISER'S APPROVAL: Hongbing Lu